

**FEDERAL UNIVERSITY OF TECHNOLOGY - PARANÁ**  
**GRADUATE PROGRAM IN ELECTRICAL AND COMPUTER ENGINEERING**

**GUILHERME HEIM WEBER**

**CHARACTERIZATION OF TRANSMISSION LINES BASED ON  
FREQUENCY-DOMAIN AND TIME-DOMAIN MEASUREMENT  
TECHNIQUES**

**MASTER THESIS**

**CURITIBA**

**2018**

**GUILHERME HEIM WEBER**

**CHARACTERIZATION OF TRANSMISSION LINES BASED ON  
FREQUENCY-DOMAIN AND TIME-DOMAIN MEASUREMENT  
TECHNIQUES**

Master thesis submitted to the Graduate Program in Electrical and Computer Engineering of Federal University – Paraná, as a partial requirement for the degree of Master of Science – Concentration Area: Automation and Systems Engineering.

Advisor: Prof. Marco José da Silva, Dr.

Co-advisor: Prof. Cicero Martelli, Dr.

**CURITIBA**

**2018**

Dados Internacionais de Catalogação na Publicação

---

W374c  
2018 Weber, Guilherme Heim  
Characterization of transmission lines based on frequency-  
-domain and time-domain measurement techniques / Guilherme  
Heim Weber.-- 2018.  
86 f. : il. ; 30 cm

Disponível também via World Wide Web  
Texto em inglês com resumo em português  
Dissertação (Mestrado) - Universidade Tecnológica Federal  
do Paraná. Programa de Pós-graduação em Engenharia Elétrica  
e Informática Industrial, Curitiba, 2018  
Bibliografia: f. 81-86

1. Linhas elétricas. 2. Linhas de telecomunicação. 3. Cabos  
elétricos. 4. Condutores elétricos. 5. Cabos de telecomunicação.  
6. Engenharia elétrica - Dissertações. I. Silva, Marco José da. II.  
Martelli, Cicero. III. Universidade Tecnológica Federal do Paraná.  
Programa de Pós-Graduação em Engenharia Elétrica e  
Informática Industrial. IV. Título.

---

CDD: Ed. 23 – 621.3

Biblioteca Central da UTFPR, Câmpus Curitiba  
Bibliotecário: Adriano Lopes CRB-9/1429

## TERMO DE APROVAÇÃO DE DISSERTAÇÃO Nº 797

A Dissertação de Mestrado intitulada “**Characterization of Transmission Lines Based on Frequency-domain and Time-domain measurement techniques**” defendida em sessão pública pelo(a) candidato(a) **Guilherme Heim Weber**, no dia 21 de maio de 2018, foi julgada para a obtenção do título de Mestre em Ciências, área de concentração Engenharia de Automação e Sistemas, e aprovada em sua forma final, pelo Programa de Pós-Graduação em Engenharia Elétrica e Informática Industrial.

BANCA EXAMINADORA:

Prof(a). Dr(a). Marco José da Silva - Presidente – (UTFPR)

Prof(a). Dr(a). Eduardo Nunes dos Santos - (UTFPR)

Prof(a). Dr(a). Daniel Discini Silveira - (UFJF)

A via original deste documento encontra-se arquivada na Secretaria do Programa, contendo a assinatura da Coordenação após a entrega da versão corrigida do trabalho.

Curitiba, 21 de maio de 2018.

## ACKNOWLEDGMENTS

I would like to acknowledge Petrobras and National Agency of Petroleum, Natural Gas and Biofuels for providing financial resources for this study.

My deepest gratitude to my advisor Professor Dr. Marco José da Silva for all the effort, patience and time dedicated to me and to this work, for being my mentor through the academic research. My gratitude to co-advisor Professor Dr. Cicero Martelli and Professor Dr. Jean Cardozo, who actively participated in the development of this work. Special thanks to Professor Dr. Daniel Pipa for providing knowledge to develop the solution of the proposed method in this work.

My gratitude to my family for all the support and encouragement during the masters, especially to my parents Matias Weber and Cleís Heim who always have kept me up and have shown me the right way. Thanks to my sisters Fernanda, Katherine and Flávia for always supporting me and caring about me.

My gratitude to Gabriella Kesikowski for always being by my side and motivating me during the development of this work.

My gratitude to my friends Jean Nakatu, Eduardo Nunes, Aluísio Wrasse, Tiago Venduscolo, Guilherme Dutra, Uilian Dreyer, Rafael Daciuk, Hector Lise, Eduardo Robin and André Di Renzo, for always being by my side and providing support.

## ABSTRACT

WEBER, G. H.. **Characterization of transmission lines based on frequency-domain and time-domain measurement techniques**. 86 p. Master Thesis - Graduate Program in Electrical and Computer Engineering of Federal University of Technology – Paraná. Curitiba, 2018.

The importance of electrical cables in modern data communication and power transmission systems cannot be overstated. Efficient and secure transmission of either data or energy depends on the healthy state of electrical cables and cable networks. In many applications, the continuous monitoring of cable characteristics is required in order to guarantee system performance. In this work, different time-domain and frequency domain techniques are applied to a set of experiments to explore different means to characterize transmission lines in a comparative manner. First, two exemplary cables are analyzed by frequency domain techniques to obtain their capacities in function of different cable lengths. Results show the influence of length over channel capacity for both cables, which were compared to commercial data transmission systems. As a second part of the experiments, a chosen cascaded transmission line set is characterized in time and frequency domain. Time domain analysis based on reflectometry and transmissometry methods reveals impedance mismatches along the line and impulse response respectively. Frequency domain analysis is based on the scattering parameters and enables the extraction of the electrical parameters of the channel. Also, time domain analysis of scattering parameters can be performed by the inverse chirp  $Z$  transform, a weak approach generally based on a minimum norm solution. Since the nature of the impedance mismatches along the line is sparse, it is proposed a sparse inverse chirp  $Z$  transform, specially designed for this kind of application. The method is verified by comparing results provided by the general approach, showing promising performance through the reflection and transmission profiles obtained.

**Keywords:** inverse chirp  $Z$  transform, frequency domain analysis, scattering parameters, time domain analysis, transmission line analysis.

## RESUMO

WEBER, G. H.. **Caracterização de linhas de transmissão baseada em técnicas de medição no domínio do tempo e no domínio da frequência**. 86 f. Dissertação de Mestrado - Programa de Pós-Graduação em Engenharia Elétrica e Engenharia de Computação da Universidade Tecnológica Federal do Paraná. Curitiba, 2018.

A importância de cabos elétricos em sistemas modernos de comunicação de dados e transmissão de energia não pode ser subestimada. A transmissão segura e eficiente de dados ou energia depende da integridade dos cabos elétricos e redes de cabos. Em muitas aplicações o monitoramento contínuo das características do cabo é necessário para garantir o desempenho do sistema. Neste trabalho, diferentes técnicas no domínio do tempo e no domínio da frequência são aplicadas a um conjunto de experimentos para explorar diferentes meios para caracterizar linhas de transmissão de forma comparativa. Primeiro, dois cabos exemplares são analisados por técnicas no domínio da frequência para obter suas capacidades em função de diferentes comprimentos de cabo. Os resultados mostram a influência do comprimento sobre a capacidade do canal para ambos os cabos, os quais foram comparados a sistemas comerciais de transmissão de dados. Como segunda parte dos experimentos, um conjunto de linhas de transmissão em cascata escolhido é caracterizado no domínio do tempo e da frequência. A análise do domínio do tempo baseada em métodos de reflectometria e transmissometria revela descasamentos de impedância ao longo da linha e resposta ao impulso, respectivamente. A análise no domínio da frequência é baseada nos parâmetros de espalhamento e permite a extração dos parâmetros elétricos do canal. Além disso, a análise no domínio do tempo dos parâmetros de espalhamento pode ser realizada pela transformada inversa chirp Z, uma abordagem fraca geralmente baseada em uma solução de norma mínima. Uma vez que a natureza dos descasamentos de impedância ao longo da linha é esparsa, propõe-se uma transformada inversa chirp Z esparsa, especialmente projetada para este tipo de aplicação. O método é verificado comparando-se os resultados fornecidos pela abordagem geral, mostrando desempenho promissor através dos perfis de reflexão e transmissão obtidos.

**Palavras-chave:** transformada inversa chirp  $Z$ , análise no domínio da frequência, parâmetros  $S$ , análise no domínio do tempo, análise de linhas de transmissão.



## LIST OF FIGURES

Figure 1 – Transmission line lumped model: (a) voltage and current definitions; (b) lumped-element equivalent circuit (POZAR, 2005). .....	26
Figure 2 - Transmission line terminated in a load impedance $Z_L$ (POZAR, 2005).....	29
Figure 3 - Locations of maximum and minimum standing wave values along the line toward the generator (IDA, 2015). .....	32
Figure 4 - Two-port network model for system connected to a source and load. Adapted from (BEGOVIĆ; SKALJO; GORAN, 2013).....	33
Figure 5 - Different shapes of reflections and their meanings (AGILENT TECHNOLOGIES, 2012). .....	37
Figure 6 - Scattering parameters measurement topology for 2-port network.....	39
Figure 7 - Chirp Z Transform: spiral contour in the Z plane. Adapted from (RABINER; SCHAFER; RADER, 1969). .....	41
Figure 8 – Two-port network - $ABCD$ matrix representation. ....	42
Figure 9 - Two-port networks in cascaded connection.....	43
Figure 10 – Frequency selective fading channel (GOLDSMITH, 2005). ....	45
Figure 11 - Block diagram of basic OFDM system. Adapted from (BAHAI; SALTZBERG; ERGEN, 2004). .....	47
Figure 12 –Cables selected for analysis: CAT5e UTP line (a) and flexible stranded two-wire copper 1.5 mm <sup>2</sup> (b). .....	51
Figure 13 - Channel set chosen to be characterized in time and frequency domain...	52
Figure 14 - Block diagram for the channel analysis proposed.....	53
Figure 15 – Time domain measurements scenario: reflectometry profile acquisition (a) and transmissometry profile acquisition (b).....	57
Figure 16 - Frequency response of the twisted-pair line for the different length sets, in dB.....	59
Figure 17 - Channel capacity and performance of the twisted-pair channel. ....	60
Figure 18 - Frequency response of the two-wire line, in dB.....	61
Figure 19 - Channel capacity and performance of the two-wire channel. ....	62

Figure 20 - TDR profiles of the channel under test in direct perspective using different pulse widths and different terminations. (a) presents the profiles obtained with the pulse 1.5 ns wide for open, short and load termination, (b) the profile obtained with the pulse 5 ns wide for each termination, and (c) the profiles using the pulse 10 ns wide. The y axis represents the magnitude of the reflection coefficients along the channel over time.....	64
Figure 21 - TDR profiles of the channel under test in reverse perspective using different pulse widths and different terminations. (a) shows the profiles obtained with the pulse 1.5 ns wide for open, short and load termination, (b) the profile obtained with the pulse 5 ns wide for each termination, and (c) the profiles using the pulse 10 ns wide. The y axis represents the magnitude of the reflection coefficients along the channel, given in time (x axis). .....	66
Figure 22 - Impulse response of the channel under analysis. (a) depicts the response considering the propagation through the direct perspective, while (b) for the contrary perspective.....	68
Figure 23 - $S_{21}$ parameter acquired for the analysis of the channel under test. (a) depicts the magnitude of the parameter, in dB. (b) presents its angle over the frequency, in rad.....	69
Figure 24 - $S_{11}$ parameter acquired for the analysis of the channel under test. (a) depicts the magnitude of the parameter, in dB. (b) presents its angle over the frequency, in rad.....	70
Figure 25 - Analysis of the parameters $S_{11}$ and $S_{22}$ in time domain, given by the conversion performed by ICZT and Sparse ICZT, in comparison to the TDR profile acquired. (a) is related to the direct perspective of the channel, whereas (b) to the reverse perspective.....	71
Figure 26 - Analysis of the parameters $S_{21}$ and $S_{12}$ in time domain, presenting results of the conversion performed by ICZT and Sparse ICZT, in comparison to the TDR profile acquired. (a) presents the parameter $S_{21}$ in time domain, related to the direct perspective propagation. (b) presents the parameter $S_{12}$ in time domain, related to the reverse perspective propagation.....	74
Figure 27 - Characteristic impedance of the cascaded transmission line under analysis calculated from the scattering parameters acquired.....	75

Figure 28 - Propagation constant calculated from the scattering parameters acquired of the mixed channel. The attenuation constant alpha (a) (real part of the propagation constant) increases with the frequency, standing near to 0.017 at 100 MHz. The phase constant beta (b) (imaginary part) varies periodically following the length of the channel under test. ....	76
Figure 29 - Distributed parameters calculated for the channel under analysis. (a) depicts the distributed resistance given in $\Omega.m^{-1}$ , (b) the distributed inductance in $\mu H.m^{-1}$ , (c) the distributed conductance in $m S.m^{-1}$ , and (d) the distributed capacitance in $p F.m^{-1}$ .....	77
Figure 30 - Frequency response of the channel under analysis, in dB.....	78

## LIST OF TABLES

Table 1 - Comparison of capacities obtained for the two cables at 10 m and 100 m long.....	63
Table 2 - Correlation between reflections of TDR profiles in both perspectives. ....	67
Table 3 - Correlation between the scattering parameters $S_{11}$ and $S_{22}$ in time domain, obtained by ICZT and Sparse ICZT, and TDR profiles. ....	72
Table 4 - Maximum relative errors for the correlation between the scattering parameters $S_{11}$ and $S_{22}$ in time domain, obtained by ICZT and Sparse ICZT, and TDR profiles, taking ICZT method as reference.....	73
Table 5 - Channel capacity (Mbps) calculated in function of the channel frequency response and noise level.....	78

## NOMENCLATURE

ADSL	Assymetric Digital Subscriber Line
AV	Audio Video
AWGN	Additive White Gaussian Noise
BPSK	Binary Phase Shift Keying
CAT5e	ANSI/TIA/EIA-568-A 5e Cable Category
CSMA/CA	Carrier Sense Multiple Acces / Collision Avoidance
CZT	Chirp Z Transform
DAB	Digital Audio Broadcasting
DFT	Discrete Fourier Transform
DMT	Discrete Multitone
DSL	Digital Subscriber Line
DVB	Digital Video Broadcasting
FDR	Frequency Domain Reflectometry
FFT	Fast Fourier Transform
FISTA	Fast Iterative Shrinkage-Thresholding Algorithm
HF	High Frequency (3 MHz to 30 MHz)
ICZT	Inverse Chirp Z Transform
IFFT	Inverse Fast Fourier Transform
IS	Impedance Spectroscopy
ISI	Intersymbol Interference
ITU	International Telecommunications Union
MAC	Media Access Control
MF	Medium Frequency (300 kHz to 3 MHz)
MIMO	Multiple Input Multiple Output
MPDU	MAC Protocol Data Unit
OFDM	Orthogonal Frequency Domain Multiplexing
PBs	PHY Blocks
PHY	Physical layer
PLC	Power Line Communication

PPDU	PHY Protocol Data Unit
PSD	Power Spectrum Density
QAM	Quadrature Amplitude Modulation
QoS	Quality of Service
SHF	Super High Frequency (3GHz to 30 GHz)
SISO	Single Input Single Output
SNR	Signal-to-Noise Ratio
SOLT	Short - Open - Load - Through
TCC	Turbo Convolutional Code
TCP/IP	Transmission Control Protocol / Internet Protocol
TDMA	Time Division Multiple Access
TDR	Time Domain Reflectometry
TDT	Time Domain Transmissometry
UHF	Ultra High Frequency (300 MHz to 3 GHz)
VHF	Very High Frequency (30 MHz to 300 MHz)
VNA	Vector Network Analyzer
WLAN	Wireless Local Area Network
WMAN	Wireless Metropolitan Area Network

## LIST OF SYMBOLS

$\alpha$	Attenuation Constant	Np/m
$\mathcal{T}$	Shrinkage operator	
$\tau$	Channel propagation delay	
$A$	ABCD parameter	
$A_0$	CZT sweeping starting radius in Z plane	
$a_0$	Length dependent attenuation parameter	
$a_1$	Length and frequency dependent attenuation parameter	
$A_{CZT}$	CZT sweeping starting point in Z plane	
$B$	ABCD parameter	
$BW$	Signal bandwidth	Hz
$C$	Distributed Capacitance	F/m
$c$	Speed of light	
$C_{ABCD}$	ABCD parameter	
$C_{CZT}$	CZT matrix operator	
$C_{\max}$	Channel capacity	bps
$C_T$	Total transmission line Capacitance	F
$d$	Total line length	m
$D$	ABCD parameter	
$D_m$	Mismatch location	m
$e$	Euler's constant	
$f$	Frequency	Hz
$f(x)$	Composite convex cost function	
$G$	Distributed Conductance	S/m
$G_T$	Total transmission line Conductance	S
$H(\omega)$	Transmission line transfer function	
$I$	Current propagating wave	A
$i(z,t)$	Current in function of length and time	A
$I_1$	Total current at the port 1 in ABCD model	A
$I_2$	Total current at the port 2 in ABCD model	A

$I_3$	Total current at the port 3 in ABCD model	A
$I_L$	Current at the load	A
$j$	Imaginary Unit	
$k$	Step number for the proximal regularization solution	
$k_f$	Exponent of the attenuation factor	
$k_s$	Convergence order parameter related to the number of steps	
$L$	Distributed Inductance	H/m
$l$	Length referred to the load	m
$L_B$	Blind spot length	m
$l_{max}$	Location of maximum value of voltage wave (in units of wave length)	$\lambda$
$l_{min}$	Location of minimum value of voltage wave (in units of wave length)	$\lambda$
$L_T$	Total transmission line Inductance	H
$N$	Additive white Gaussian noise power level	W
$O$	Convergence order parameter	
$R$	Distributed Resistance	$\Omega/m$
$RL$	Return loss	dB
$R_T$	Total transmission line Resistance	$\Omega$
$S$	Average signal power	W
$S$	Scattering parameters matrix	
$S_{11}$	Input reflection coefficient with matched output	
$S_{12}$	Reverse transmission coefficient with matched input	
$S_{21}$	Forward transmission coefficient with matched output	
$S_{22}$	Output reflection coefficient with matched input	
$SWR$	Standing Wave Ratio	
$t$	Time	s
$t_k$	Step size for proximal regularization solution	
$t_{Resolution}$	TDR time resolution	s
$t_{width}$	Interrogation pulse width	s
$V$	Voltage propagating wave	V



$V^-$	Backward propagating wave	V
$v(z,t)$	Voltage in function of length and time	V
$V^+$	Forward propagating wave	V
$V_0^-$	Voltage wave propagating through negative $z$ direction	V
$V_0^+$	Voltage wave propagating through positive $z$ direction	V
$V_1$	Total voltage at the port 1 in ABCD model	V
$V_2$	Total voltage at the port 2 in ABCD model	V
$V_3$	Total voltage at the port 3 in ABCD model	V
$V_L$	Voltage at the load	V
$v_p$	Phase velocity	m/s
$V_{rel}$	Relative speed of the signal on the channel	
$W$	CZT parameter that defines how the contour spirals over the Z plane	
$W_0$	CZT sweeping rate	
$X(k)$	M points resulting sequence ( $0 \leq k \leq M-1$ )	
$x(n)$	N points primary sequence ( $0 \leq n \leq N-1$ )	
$x_0$	Initial value for the solution sequence $x_k$	
$x_k$	Solution sequence for proximal regularization solution	
$z$	Line length	m
$Z(l)$	Line impedance at any point	$\Omega$
$Z_0$	Characteristic impedance of an equipment	$\Omega$
$Z_C$	Characteristic Impedance	$\Omega$
$Z_d$	Local discontinuity Characteristic Impedance	$\Omega$
$Z_L$	Load impedance	$\Omega$
$Z_{open}$	Input impedance for a transmission line terminated in open circuit	$\Omega$
$Z_S$	Source impedance	$\Omega$
$Z_{short}$	Input impedance for a transmission line terminated in short circuit	$\Omega$
$\Delta F$	Frequency span	Hz
$\Delta z$	Infinitesimal Length	m
$\Gamma_L$	Reflection coefficient	

$\Gamma(l)$	Reflection coefficient at any point	
$\beta$	Phase Constant	rad/m
$\gamma$	Propagation Constant	
$\varphi_0$	CZT sweeping angle step size	rad
$\lambda$	Wave length	m
$\lambda_{CZT}$	Regularization parameter of L2-L1 minimization problem solution	
$\mathbb{R}$	Set of real numbers	
$\theta_0$	CZT sweeping starting angle in Z plane	rad
$\theta_\Gamma$	Reflection coefficient phase angle	rad
$\theta_{\Gamma(l)}$	Reflection coefficient at any point phase angle	rad
$\rho$	Reflection coefficient	
$\omega$	Angular Frequency	rad/s

## CONTENTS

<b>1 INTRODUCTION .....</b>	<b>21</b>
1.1 MOTIVATION .....	21
1.2 OBJECTIVES.....	23
1.2.1 General Objective.....	23
1.2.2 Specific Objectives .....	23
1.3 STRUCTURE.....	24
<b>2 THEORETICAL BACKGROUND.....</b>	<b>25</b>
2.1 TRANSMISSION LINES .....	25
2.1.1 The Lumped Model.....	25
2.1.2 The Load Reflection Coefficient .....	29
2.1.3 Line Impedance and the Generalized Reflection Coefficient.....	29
2.1.4 The Terminated Lossless Transmission Line.....	30
2.1.5 Transmission Line Transfer Function .....	33
2.2 NETWORK ANALYSIS.....	33
2.2.1 Time Domain Reflectometry .....	34
2.2.2 Scattering Parameters .....	38
2.2.2.1 Scattering parameters in time domain.....	40
2.2.3 <i>ABCD</i> Matrix .....	42
2.2.4 Impedance Spectroscopy .....	44
2.2.5 Shannon-Hartley Theorem .....	44
2.2.6 LTI Channel Model.....	45
2.3 ORTHOGONAL FREQUENCY DIVISION MULTIPLEXING .....	46
2.3.1 Power Line Communication.....	47
2.3.1.1 HomePlug AV2 .....	48
<b>3 METHODOLOGY .....</b>	<b>50</b>
3.1 INFLUENCE OF THE LENGTH OVER THE CHANNEL CAPACITY SET	50
3.2 CHANNEL ANALYSIS THROUGH TIME DOMAIN AND FREQUENCY DOMAIN DATA .....	52

3.2.1 Frequency Domain Data Acquisition and Analysis .....	53
3.2.1.1 Sparse Inverse Chirp-Z Transform for Time Domain Analysis.....	54
3.2.2 Time Domain Data Acquisition and Analysis .....	56
<b>4 RESULTS AND DISCUSSIONS .....</b>	<b>59</b>
4.1 CHANNEL CAPACITY IN DIFFERENT LENGTHS.....	59
4.1.1 Twisted-Pair Line .....	59
4.1.2 Two-Wire Stranded Line.....	61
4.2 CHANNEL ANALYSIS IN TIME AND FREQUENCY DOMAIN .....	64
4.2.1 Time Domain Results.....	64
4.2.2 Frequency Domain Results.....	69
<b>5 CONCLUSIONS .....</b>	<b>79</b>
5.1 FUTURE WORK.....	80
<b>REFERENCES.....</b>	<b>81</b>

## 1 INTRODUCTION

### 1.1 MOTIVATION

The use of electrical cables to transmit data or energy has steadily grown in the past due to the fast expansion of the demand on energy and communication industries. Current end-consumer or industrial systems demand transmission rates greater than ever existed as well as more efficient power transmission through smaller, less susceptible to electromagnetic interference and less noise generating transmission lines.

Several applications come up with different issues such as cable attenuation, possible impedance mismatches along the channel, faults, electromagnetic susceptibility and thermal noise. Cables faults (sometimes intermittent) can cause power failure or loss of control, giving the importance of monitoring the integrity of the cables (YAMADA; HIRAI; OHKI, 2012). On the aircrafts industry, typically there are several tens of miles of wires within their structures (BLEMEL; FURSE, 2001), and wiring problems have already been identified as the likely cause of several accidents (SMITH; FURSE; GUNTHER, 2005). Among the wiring problems there are wire insulation chafing, defective connections, ticking short circuits, solid short circuits, insulation breakdown, exposed conductors and corrosion (BLEMEL; FURSE, 2001). Once placed on their designated positions such problems often cannot be identified and fixed. The mechanical structure on these kind of environments does not allow visual inspection or any direct located measuring.

In the oil industry, for example, there is a need for measuring and registering oil reservoir's characteristics of offshore wells. Subsea installations imply in some restrictions on the electrical cables for communications systems and electrical power energy distribution which supply down-hole electronics and tools (RITO et al., 2013). Hence, the development of systems like those demands a prior knowledge about the electrical parameters of existing cable structures and in some application the need for continuous monitoring of electrical cables and their current transmission performance. In a communication system for example, is essential to know the maximum possible capacity to achieve through a given channel. Current communication technologies like Orthogonal Frequency Domain Multiplexing (OFDM) and Turbo Convolutional Code (TCC) provides robust performance within 0.5 dB of Shannon's limit (ALLIANCE;

RESERVED, 2005), implying on the importance of knowing the channel capacity of a target transmission line and on the efficiency of the application at all.

This scenario opens horizons for methods for detecting faults on cable and/or its current transmission capacity. The most known and applied so far are reflectometry based methods like time-domain reflectometry (TDR), frequency-domain reflectometry (FDR) (CHING-WEN HSUE; TE-WEN PAN, 1997) (VANHAMME, 1990), time gating methods (DUNSMORE; CHENG; ZHANG, 2011), and identification of moderate reflections of cascaded circuits by transmission and reflection measurements (VEIJOLA; VALTONEN, 1988). The main idea of all those techniques consists in applying a high frequency stimulus to the line and monitor the reflected signals generated by impedance mismatches. Although their success on this field, most of reflectometry based methods have a restricted application given by certain assumptions such as small amplitudes for the reflections (VEIJOLA; VALTONEN, 1988) (VANHAMME, 1992) or prior knowledge about the line under test (VANHAMME, 1990). Recently a method based on a sample maximum likelihood estimator for locating and separating closely spaced reflections with high magnitude has been proposed (ZYARI; ROLAIN, 2016), at the expense of an increase in complexity of the model yet. Another technique for characterizing transmission lines is called impedance spectroscopy (IS), which consists in measuring the impedance of the line under test in a given frequency spectrum with one end terminated in short and open circuit. From these measurements it is calculated the parameters characteristic impedance and propagation constant, and from these the primary ones, composing a model of the line over the frequency spectrum acquired (SHI; KANOUN, 2013). Impedance spectroscopy also enables the analysis of the line in time domain, allowing to identify faults along it .(QINGHAI SHI; KANOUN, 2015).

Despite of its simple concept, time-domain methods come up with limitations on signal detection, implying a restriction on the application to monitor weak impedance mismatches or at high noisy and high attenuation systems (AGILENT TECHNOLOGIES, 2012). Moreover, they require ideal open and short terminations, which are difficult to achieve over a broadband frequency range. Due to electric field fringing at high frequencies, open circuit terminations cause stray capacitance, and short circuit terminations introduce additional inductance to the line (PAPAZYAN et al., 2004). These problems on measurements are also related to the IS method.

Facing all these facts, the concept of travelling waves for the analysis of transmission lines becomes an attractive alternative. The scattering parameters, basis

of this analysis, do not depend on terminations but only on incident, scattered and reflected waves over the network. The parameters are acquired on frequency domain at one frequency at a time using a vector network analyzer, which provides high signal-to-noise ratio and high frequency resolution over a wide bandwidth. In addition, the analysis of the network in time domain through the scattering parameters is possible, and is given by the conversion through the Inverse Chirp Z Transform (RABINER; SCHAFER; RADER, 1969), first proposed in 1969 and already used by commercial instruments.

## 1.2 OBJECTIVES

### 1.2.1 General Objective

Facing the importance of studying and monitoring electrical cables and cables networks, it is aims of this work to explore techniques to characterize electrical cables, evaluating their behavior through time and frequency domain analysis. The possible scenario of application were for the oil industry in subsea and downhole systems, in which non-optimal electrical connection exists, e.g. no impedance match and different cable types along same line.

### 1.2.2 Specific Objectives

In order to evaluate the influence of the length of a channel over its capacity, two different types of cable were chosen to be the channels under test, exemplary test beds. Through the analysis of the scattering parameters acquired from these cables in different lengths, their capacities are evaluated in function of different noise levels, following the Shannon-Hartley's theorem. Then, channel capacity curves are compared to the performance of a commercial communication system running over the channel at its different lengths, in a way to evaluate the working noise level of the modems used.

As a second specific objective is evaluating the electrical parameters of a given transmission line in time and frequency domain. Through time domain reflectometry and transmissometry methods a clear view about the changes on the impedance along

the line can be achieved, as well its length and impulse response. Through scattering parameters in frequency domain, the primary and secondary parameters of the channel under test can be acquired and calculated. The presented work also aims to explore means to convert frequency domain parameters to time domain, enabling the same analysis obtained from reflectometry and transmissometry methods.

### 1.3 STRUCTURE

The presented work is organized in five sections, as follows: the second section (theoretical background) presents a brief theory about transmission lines and network analysis, going from their electrical characteristics and behavior to methods for acquiring their electrical parameters and characterizing them in time and frequency domain; the third section (methodology) describes two different sets of experiments proposed, being the first one designed to relate the influence of the channel length to its capacity, and the second one a proposed set of analysis to characterize a given channel in frequency and time domain; the fourth section presents results and discussions; the fifth section concludes this work and describes proposed future research.



## 2 THEORETICAL BACKGROUND

### 2.1 TRANSMISSION LINES

Transmission lines are structures in which electric energy and signals propagate from a source to a load. From connections between a transmitter and an antenna, between computers in a network, to the ones between a hydroelectric generating plant and a substation several hundred kilometers away are some examples of typical transmission lines found nowadays (HAYT; BUCK, 2011).

Circuit theory and transmission lines theory differ essentially by the electrical size involved. Physical dimensions in circuit theory are much smaller than the electrical wavelength of the propagating signal, so the amplitude along the line is treated as constant. In the transmission line scenario, the line length can be a fraction or many times the electrical wavelength, so the amplitude and phase of the wave vary along the line and thus are not negligible anymore (POZAR, 2005).

The characterization of a transmission line is given by parameters which describe its electrical properties as a function of the constructive characteristics of the line and the electrical properties of the component materials, as well of the transmitting signal frequency.

#### 2.1.1 The Lumped Model

While ordinary circuit analysis deals with lumped elements, where voltage and current do not vary appreciably over the physical dimension of the elements, a transmission line is a distributed parameter network, where voltages and currents vary in magnitude and phase over its length. The distributed parameters of a transmission line refer to the representation of electrical characteristics in a length unit. This idea gave rise to the *RLGC* model, which consists of a minimalist model that represents a transmission line with lumped elements.  $R$  represents the series resistance due to the finite conductivity of the individual conductors per unit length in  $\Omega/m$ , for both conductors.  $L$  represents the series inductance per unit length of the two conductors, in  $H/m$ .  $G$  represents the shunt conductance per unit length due to dielectric loss in the material between the conductors, given in  $S/m$ .  $C$  represents the shunt capacitance

per unit length, due to the close proximity of the two conductors, in  $F/m$ . An infinitesimal length  $\Delta z$  of the line represented by two-wire conductors in Figure 1.a, can be modeled with lumped elements (POZAR, 2005), as shown in Figure 1.b.

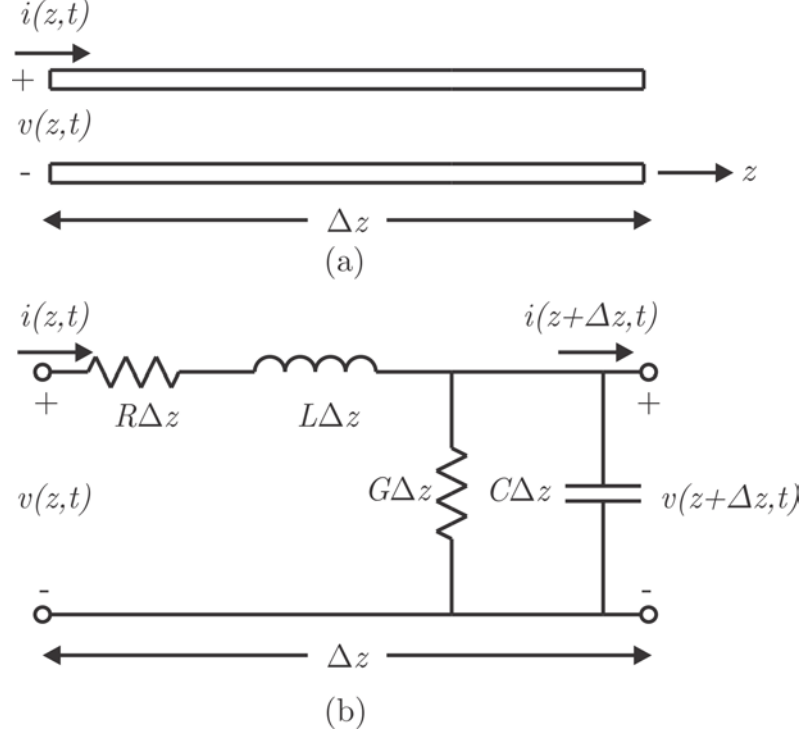


**Figure 1 – Transmission line lumped model: (a) voltage and current definitions; (b) lumped-element equivalent circuit (POZAR, 2005).**

Applying Kirchhoff's voltage and current laws to the lumped-element equivalent circuit, one obtains (2.1) and (2.2) respectively:

$$v(z,t) - R\Delta z i(z,t) - L\Delta z \frac{\partial i(z,t)}{\partial t} - v(z + \Delta z,t) = 0, \quad (2.1)$$

$$i(z,t) - G\Delta z v(z + \Delta z,t) - C\Delta z \frac{\partial v(z + \Delta z,t)}{\partial t} - i(z + \Delta z,t) = 0. \quad (2.2)$$

Taking the limit as  $\Delta z \rightarrow 0$  after dividing (2.1) and (2.2) by  $\Delta z$  one obtains the differential equations (2.3) and (2.4):

$$\frac{\partial v(z,t)}{\partial z} = -Ri(z,t) - L \frac{\partial i(z,t)}{\partial t}, \quad (2.3)$$

$$\frac{\partial i(z,t)}{\partial z} = -Gv(z,t) - C \frac{\partial v(z,t)}{\partial t}. \quad (2.4)$$

Equations (2.3) and (2.4) are known as the telegrapher equations, being the time domain form of the transmission line equations (POZAR, 2005). Considering the steady-state condition with cosine-based phasors these equations simplify to (2.5) and (2.6) as two coupled first-order differential equations:

$$\frac{dV(z)}{dz} = -(R + j\omega L)I(z) , \quad (2.5)$$

$$\frac{dI(z)}{dz} = -(G + j\omega C)V(z) . \quad (2.6)$$

Aiming to obtain separate equations for  $V(z)$  and  $I(z)$ , one substitutes  $I(z)$  from equation (2.5) into (2.6) and  $V(z)$  from (2.6) into (2.5). From (2.5) one obtains (2.7):

$$I(z) = -\frac{dV(z)}{dz} \frac{1}{[R + j\omega L]} . \quad (2.7)$$

Substituting (2.7) in (2.6) leads to (2.8):

$$\frac{d^2V(z)}{dz^2} - V(z)[G + j\omega C][R + j\omega L] = 0 , \quad (2.8)$$

and similarly, substituting  $V(z)$  from (2.6) into (2.5) leads to :

$$\frac{d^2I(z)}{dz^2} - I(z)[G + j\omega C][R + j\omega L] = 0 . \quad (2.9)$$

These two wave equations for  $V(z)$  and  $I(z)$  can be rewritten as (2.10) and (2.11):

$$\frac{d^2V(z)}{dz^2} - \gamma^2 V(z) = 0 , \quad (2.10)$$

$$\frac{d^2I(z)}{dz^2} - \gamma^2 I(z) = 0 , \quad (2.11)$$

being  $\gamma$  the propagation constant, a complex number that rules how the wave propagates along the line, defined by the relation (2.12):

$$\gamma = \alpha + j\beta = \sqrt{(R + j\omega L)(G + j\omega C)} . \quad (2.12)$$

$\alpha$ , the real part of  $\gamma$ , is the attenuation coefficient given in Nepers per meter, while  $\beta$ , the imaginary part, is the phase constant given in radians per meter. The travelling wave solution for (2.5) and (2.6) is given then by (2.13) and (2.14):

$$V(z) = V_0^+ e^{-\gamma z} + V_0^- e^{\gamma z} [V] , \quad (2.13)$$

$$I(z) = I_0^+ e^{-\gamma z} + I_0^- e^{\gamma z} [A] , \quad (2.14)$$

where  $e^{-\gamma z}$  denotes the wave propagation in the  $+z$  direction, while  $e^{\gamma z}$  the wave propagation in the  $-z$  direction.  $V_0^+$  and  $V_0^-$  are the amplitudes of the voltage waves propagating in the positive and negative  $z$  directions, respectively. The same designation is used for current waves propagating  $I_0^+$  and  $I_0^-$ .

The relationship between the voltage wave propagation and the current wave propagation defines the characteristic impedance  $Z_c$  (2.15):

$$\frac{V_0^+}{I_0^+} = \frac{-V_0^-}{I_0^-} = Z_c , \quad (2.15)$$

which can be related to the electrical parameters of the line substituting the general solution from (2.13) and (2.14) into the transmission line relation in (2.5) and (2.6). From (2.5) one obtains (2.16):

$$\frac{d(V_0^+ e^{-\gamma z} + V_0^- e^{\gamma z})}{dz} = -(I_0^+ e^{-\gamma z} + I_0^- e^{\gamma z})[R + j\omega L] . \quad (2.16)$$

Solving the derivatives leads to (2.17):

$$-\gamma V_0^+ e^{-\gamma z} + \gamma V_0^- e^{\gamma z} = -(I_0^+ e^{-\gamma z} + I_0^- e^{\gamma z})[R + j\omega L] . \quad (2.17)$$

Similarly, substituting (2.14) into (2.6) and solving the derivatives one obtains (2.18):

$$-\gamma I_0^+ e^{-\gamma z} + \gamma I_0^- e^{\gamma z} = -(V_0^+ e^{-\gamma z} + V_0^- e^{\gamma z})[G + j\omega C] . \quad (2.18)$$

Considering only the forward propagating wave ( $V_0^- = I_0^- = 0$ ) in equations (2.17) and (2.18) one obtains (2.19):

$$\begin{aligned} -\gamma V_0^+ e^{-\gamma z} &= -I_0^+ e^{-\gamma z} [R + j\omega L] \\ -\gamma I_0^+ e^{-\gamma z} &= -V_0^+ e^{-\gamma z} [G + j\omega C] , \end{aligned} \quad (2.19)$$

leading to the rewritten for characteristic impedance as (2.20):

$$Z_c = \frac{V_0^+}{I_0^+} = \frac{R + j\omega L}{\gamma} = \frac{\gamma}{G + j\omega C} . \quad (2.20)$$

Substituting  $\gamma$  from (2.12) in (2.20) one obtains (2.21) (IDA, 2015):

$$Z_c = \sqrt{\frac{R + j\omega L}{G + j\omega C}} \quad [\Omega] . \quad (2.21)$$

The same relation for the characteristic impedance can be found by considering only the backward propagating wave ( $V_0^+ = I_0^+ = 0$ ).

The current wave propagation (2.14) can be rewritten as (2.22):

$$I(z) = \frac{V_0^+}{Z_c} e^{-\gamma z} - \frac{V_0^-}{Z_c} e^{\gamma z} . \quad (2.22)$$

The wavelength on the line is related with the phase constant as (2.23):

$$\lambda = \frac{2\pi}{\beta} , \quad (2.23)$$

and the phase velocity is given by the relation (2.24)

$$v_p = \frac{\omega}{\beta} = \lambda f . \quad (2.24)$$

Another parameter commonly used is the electrical length of the line, given by  $\beta z$  in radians (IDA, 2015).

### 2.1.2 The Load Reflection Coefficient

Considering a load connected to a transmission line and located at  $l=0$  ( $l$  equal to the maximum  $z$  or the length of the line) as shown in Figure 2:

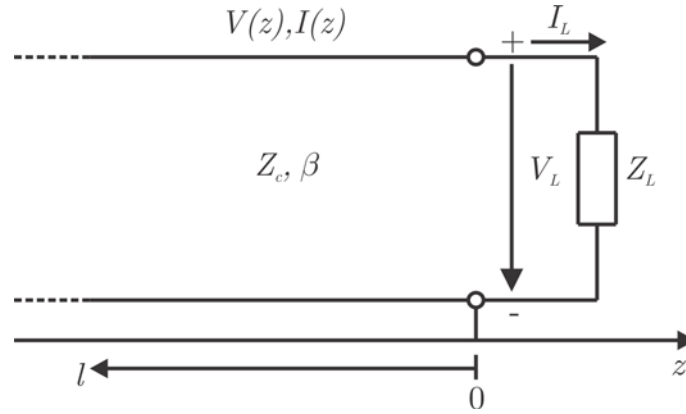


Figure 2 - Transmission line terminated in a load impedance  $Z_L$  (POZAR, 2005).

Recalling the definition of  $Z_C$  in (2.15) and, the load impedance will be given by the relation between the total voltage and current propagating through a transmission line as (2.25):

$$Z_L = \frac{V(0)}{I(0)} = \frac{V^+ + V^-}{I^+ + I^-} = \frac{V^+ + V^-}{V^+ / Z_c - V^- / Z_c} = Z_c \frac{V^+ + V^-}{V^+ - V^-} , \quad (2.25)$$

being the total voltage and current the sum of the forward and backward propagating waves. At the condition of matching between load and line, there will not exist a backward propagating wave ( $V^-=0$ ) since the load impedance equals to the characteristic impedance of the line.

Therefore, the backward propagating wave will only exist when  $Z_L \neq Z_C$ , due to the reflection of the forward propagating wave at the load. The relation between reflection  $V^-$  and forward  $V^+$  waves defines the load reflection coefficient as (2.26):

$$\Gamma_L = \frac{V^-}{V^+} = \frac{Z_L - Z_c}{Z_L + Z_c} = |\Gamma_L| e^{j\theta_\Gamma} , \quad (2.26)$$

being a complex number where  $\theta_\Gamma$  is the phase angle of the reflection coefficient.

### 2.1.3 Line Impedance and the Generalized Reflection Coefficient

Line impedance refers to the impedance at any point on the line. It can be obtained dividing the total voltage at any point on the line (2.13) by the total current also at

any point on the line (2.14). Rewriting the current in terms of voltage and characteristic impedance and using the concept of load reflection coefficient presented in (2.26) leads to (2.27) and (2.28)

$$V(l) = V^+(e^{\gamma l} + \Gamma_L e^{-\gamma l}) \text{ [V]} , \quad (2.27)$$

$$I(l) = \frac{V^+}{Z_0}(e^{\gamma l} - \Gamma_L e^{-\gamma l}) \text{ [A]} . \quad (2.28)$$

Dividing  $V(l)$  by  $I(l)$  to obtain the line impedance at any point  $Z(l)$  one obtains (2.29)

$$Z(l) = \frac{V(l)}{I(l)} = Z_c \frac{(e^{\gamma l} + \Gamma_L e^{-\gamma l})}{(e^{\gamma l} - \Gamma_L e^{-\gamma l})} \text{ [\Omega]} . \quad (2.29)$$

Using the identities  $(e^{\gamma l} + e^{-\gamma l})/2 = \cosh \gamma l$  and  $(e^{\gamma l} - e^{-\gamma l})/2 = \sinh \gamma l$ , the line impedance equation can also be rearranged as (2.30)

$$Z(l) = Z_0 \frac{Z_L + Z_c \tanh \gamma l}{Z_0 + Z_c \tanh \gamma l} \text{ [\Omega]} . \quad (2.30)$$

Thus, the reflection coefficient at point  $l$  on the line can be achieved by (2.31)

$$\Gamma(l) = \frac{V^-(l)}{V^+(l)} = \frac{V^+ \Gamma_L e^{-\gamma l}}{V^+ e^{\gamma l}} = \frac{\Gamma_L e^{-\gamma l}}{e^{\gamma l}} = \Gamma_L e^{-2\gamma l} , \quad (2.31)$$

which can be rewritten as (2.32)

$$\Gamma(l) = \Gamma_L e^{-2\gamma l} = |\Gamma_L| e^{-2\alpha l} e^{j\theta_r} e^{-j2\beta l} . \quad (2.32)$$

To distinguish it from the load reflection coefficient  $\Gamma_L$ ,  $\Gamma(l)$  is called the generalized reflection coefficient (IDA, 2015). On a general lossy line this coefficient has an amplitude  $|\Gamma_L|$  at the load which decays exponentially as  $z$  increases (toward the generator), and a phase varying linearly along  $l$  set by the phase constant  $\beta$  as (2.33)

$$\phi_{\Gamma(l)} = \theta_r - 2\beta l \text{ [rad]} . \quad (2.33)$$

#### 2.1.4 The Terminated Lossless Transmission Line

Considering a lossless line ( $\alpha=0$  and  $\gamma=j\beta$ ), terminated in  $Z_L$ , the voltage and current on the line becomes (2.34) and (2.35) respectively

$$V(l) = V^+(e^{j\beta l} + \Gamma_L e^{-j\beta l}) \text{ [V]} , \quad (2.34)$$

$$I(l) = \frac{V^+}{Z_0}(e^{j\beta l} - \Gamma_L e^{-j\beta l}) \text{ [A]} . \quad (2.35)$$

From (2.30) and using the identity  $\tanh(j\beta l) = j \tan(\beta l)$ , the line impedance of a lossless transmission line is given by (2.36)

$$Z(l) = Z_c \frac{Z_L + jZ_c \tan \beta l}{Z_c + jZ_L \tan \beta l} = Z_c \frac{Z_L \cos \beta l + jZ_c \sin \beta l}{Z_c \cos \beta l + jZ_L \sin \beta l} [\Omega] , \quad (2.36)$$

and the generalized reflection coefficient by (2.37)

$$\Gamma(l) = \Gamma_L e^{-j2\beta l} = |\Gamma_L| e^{j\theta_\Gamma} e^{-j2\beta l} = \Gamma_L (\cos(\theta_\Gamma - 2\beta l) - j \sin(\theta_\Gamma - 2\beta l)) . \quad (2.37)$$

The phase rules how the voltage and current vary along the line, resulting in maxima and minima points, as well for the reflection coefficient. Rearranging the terms in (2.34) and (2.35) one obtains the maximum and minimum values for voltage (2.38)

$$\begin{aligned} V_{\max} &= |V^+| (1 + |\Gamma(l)|) \quad [\text{V}] \\ V_{\min} &= |V^+| (1 - |\Gamma(l)|) \quad [\text{V}] , \end{aligned} \quad (2.38)$$

and for current (2.39)

$$\begin{aligned} I_{\max} &= \frac{V_{\max}}{|Z_c|} = \frac{|V^+|}{|Z_c|} (1 + |\Gamma(l)|) \quad [\text{A}] \\ I_{\min} &= \frac{V_{\min}}{|Z_c|} = \frac{|V^+|}{|Z_c|} (1 - |\Gamma(l)|) \quad [\text{A}] \end{aligned} . \quad (2.39)$$

A mismatched load implies a not full power transfer from the generator to the load. This “loss” is called return loss ( $RL$ ) (POZAR, 2005), defined in dB by (2.40)

$$RL = -20 \log |\Gamma| \quad [\text{dB}] . \quad (2.40)$$

When there is no reflection ( $\Gamma=0$  matched load), the return loss is equal to  $-\infty$  dB, whereas total reflection ( $|\Gamma|=1$ ) gives a return loss of 0 dB.

Another term used in microwave circuit analysis is called standing wave ratio (SWR), defined as the ratio between the maximum and minimum voltage (or current) as (2.41)

$$\text{SWR} = \frac{V_{\max}}{V_{\min}} = \frac{I_{\max}}{I_{\min}} = \frac{1 + |\Gamma(l)|}{1 - |\Gamma(l)|} \quad [\text{dimensionless}] . \quad (2.41)$$

The SWR is dimensionless and varies between 1 (no reflection) and  $\infty$  (total reflection).

Rewriting the equations (2.34) and (2.35) for the voltage and current anywhere on the line, but now expanding the term  $\Gamma_L$  one obtains (2.42) and (2.43)

$$V(l) = V^+ e^{j\beta l} (1 + \Gamma_L e^{-j2\beta l}) = V^+ e^{j\beta l} (1 + |\Gamma_L| e^{j\theta_\Gamma} e^{-j2\beta l}) \quad [\text{V}] , \quad (2.42)$$

$$I(l) = \frac{V^+}{Z_0} e^{j\beta l} (1 - \Gamma_L e^{-j2\beta l}) = \frac{V^+}{Z_0} e^{j\beta l} (1 - |\Gamma_L| e^{j\theta_\Gamma} e^{-j2\beta l}) \quad [\text{A}] . \quad (2.43)$$

At the load, voltage and current are given by setting  $l = 0$  as (2.44)

$$\begin{aligned} V_L &= V^+(1 + |\Gamma_L| e^{j\theta_\Gamma}) \text{ [V]} \\ I_L &= \frac{V^+}{Z_0}(1 - |\Gamma_L| e^{j\theta_\Gamma}) \text{ [A]} \end{aligned} \quad (2.44)$$

Analyzing equations (2.42) and (2.43), voltage wave assumes minimum values at the phase (2.45)

$$\theta_\Gamma - 2\beta l = -(2n + 1)\pi, \quad n = 0, 1, 2, \dots \quad (2.45)$$

Thus, using the identity  $\lambda = 2\pi/\beta$ , the locations for minimum values of voltage can be obtained by the relation (2.46)

$$l_{\min} = \frac{\lambda}{4\pi}(\theta_\Gamma + (2n + 1)\pi) \text{ [\lambda]}, \quad n = 0, 1, 2, \dots \quad (2.46)$$

which indicates the distance in units of wavelength. Maximum values occur at a distance of  $\lambda/4$  on each side from minimum locations as (2.47)

$$l_{\max} = \frac{\lambda}{4\pi}(\theta_\Gamma + 2n\pi) \text{ [\lambda]}, \quad n = 0, 1, 2, \dots \quad (2.47)$$

Figure 3 shows the representation of maxima and minima values for voltage and current standing waves along the line.

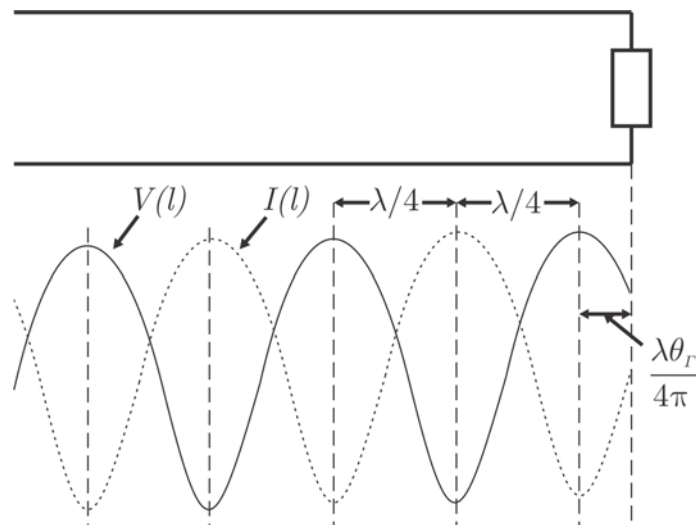


**Figure 3 - Locations of maximum and minimum standing wave values along the line toward the generator (IDA, 2015).**

Line impedance assumes maximum values at locations of voltage maxima (current minima), and minimum ones at locations of voltage minima (current maxima).



### 2.1.5 Transmission Line Transfer Function

The transfer function of a transmission line ideally terminated in  $Z_C$  is defined by the relation (2.48) (ROHLING, 2011):

$$H(\omega) = e^{-\gamma d} = e^{-\alpha d} e^{-j\beta d} , \quad (2.48)$$

with  $d$  representing the total length of the line under analysis.

Another approaching for the transfer function is relating the primary parameters of the channel to the parameters of a source and load series connected as depicted in Figure 4.

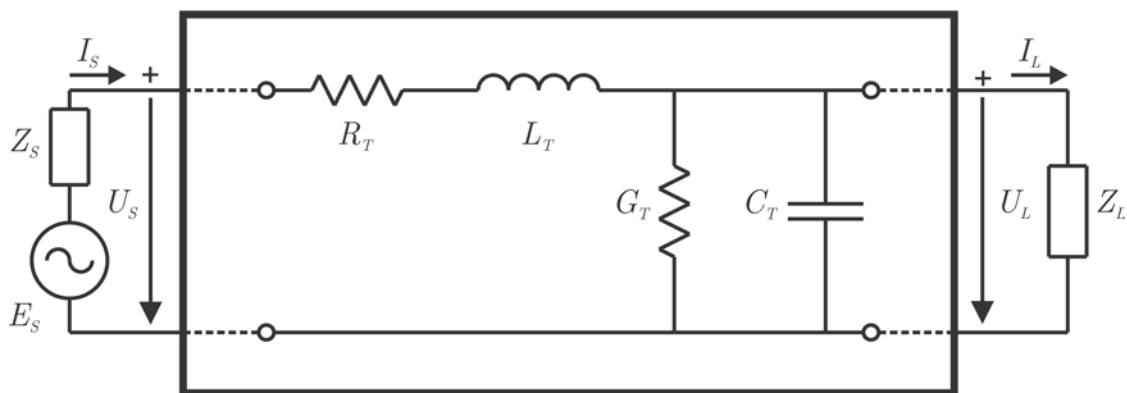


Figure 4 - Two-port network model for system connected to a source and load. Adapted from (BEGOVIĆ; SKALJO; GORAN, 2013).

The transfer function of the channel can be written as (2.49) (BEGOVIĆ; SKALJO; GORAN, 2013):

$$H(\omega) = \frac{Z_L}{Z_L + (1 + Z_L(G_T + j\omega C_T))(Z_s + (R_T + j\omega L_T))} , \quad (2.49)$$

relating the transfer function directly to the primary parameters of the channel under analysis. In this equation the primary parameters are denoted with a T overwritten, for being total values, not per unit length.

## 2.2 NETWORK ANALYSIS

This section presents strategies for characterizing wired single-input single-output (SISO) networks, starting with the simplest one: time domain reflectometry, followed by the analysis based on scattering parameters,  $ABCD$  parameters, impedance

spectroscopy and finally a channel model for linear time invariant channels aiming to accomplish the Shannon's capacity.

### 2.2.1 Time Domain Reflectometry

Time domain reflectometry (TDR) is a method introduced in the early 1960's for evaluating a transmission line in time domain using a pulse generator and a broadband oscilloscope. It consists in applying a high frequency stimulus over the channel (impulse or step) and monitoring the reflected signals caused by impedance mismatches along the line, as well as by the end of the line. Magnitude of each reflection is directly related to the reflection coefficient related to the pulse generator impedance, while its location in time gives the exact location of that mismatch in the line. Once known the line propagation velocity it is possible to associate the time of each reflection gave by the TDR trace with its location in the line. The type of each discontinuity can also be identified by its response, being capacitive or inductive (AGILENT TECHNOLOGIES, 2012). Changes in impedance can be caused by faults as short-circuits, splices, open connections, taps in the cable system, deteriorated neutrals, water ingress into insulation material or joints, and high resistance connectors (HERNANDEZ-MEJIA, 2016). Compared to other measurement techniques, time domain reflectometry provides a more intuitive and direct look at the channel under analysis (AGILENT TECHNOLOGIES, 2013), it is easy to employ, test equipment are small and not expensive, analysis at low voltage and periodic testing provides historical data.

The magnitude of the reflections ( $\rho$ ) will be given by the relation between the characteristic impedance of the line  $Z_c$  and the characteristic impedance of local discontinuity  $Z_d$  as (2.50):

$$\rho = \frac{Z_d - Z_c}{Z_d + Z_c} . \quad (2.50)$$

The reflection coefficient varies from -1, meaning short circuit, to 1, meaning open circuit. The zero value represents no reflection, implying the perfect matching.

The location of each mismatch in unit of length is achieved by the relation between the time taken to the pulse travel to this location, reflect and travel back to the start of the line as (2.51):

$$D_m = \frac{v t}{2} , \quad (2.51)$$

being  $t$  the transit time,  $v_p$  the velocity of propagation and  $D_m$  the location of the mismatch. If unknown yet, the velocity of propagation can be determined using a cable of the same type of a known length, and verifying the time required for an incident pulse travel down, reflect at the end of the line in an open circuit termination and travel back to the start (AGILENT TECHNOLOGIES, 2013). The velocity of propagation is generally defined in terms of speed of light in vacuum environment, as 100 % reference. For instance, the velocity of propagation on a coaxial line RG-58U is 65.9 % (PASTERNAK, 2017), while for a CAT5e twisted pair line is about 67 % (DRAKA, 2017).

The characteristics of the pulse are very relevant to the performance of the analysis. The amplitude is defined as the peak amplitude of the TDR pulse, being the maximum value of the trace not depending on its shape. The pulse width is defined as the time that the amplitude keeps at 50 % of its peak amplitude, and is related to the resolution in time / length of the result TDR trace. The resolution is given by the relation (2.52) :

$$t_{\text{Resolution}} = \frac{t_{\text{width}}}{2} . \quad (2.52)$$

Therefore, a pulse 10 ns wide performs a TDR trace with resolution of 5 ns. Considering a line with velocity of propagation of 66%, the resolution in length is about 0.99 m. The narrower the pulse the greater the resolution of the analysis.

Despite of the easy implementation, there is an inherited drawback related to reflectometry based methods known as dead zone or a blind spot. It is generated when the channel under test is short enough in a way that an overlap occurs between the incident and the reflected wave from a fault (KWAK et al., 2008). For this reason, this phenomenon is truly relevant as it indicates the minimum cable length which can be tested. The blind spot length is directly related to the width of the incident pulse. The wider the pulse the larger the blind spot. The blind spot length  $L_B$  is equal to the resolution time converted into length once it is known the velocity of propagation in the cable as (2.53) :

$$L_B = \frac{v_p t_{\text{width}}}{2} . \quad (2.53)$$









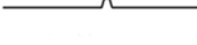



So, taking for instance the example described above where the pulse is 10 ns wide, the blind spot is 0.99 meter long. Faults located below this length will not be possible to be identified using the TDR trace. There are some solutions to work around this problem like the addition of an extension cable as the simplest one, the dual time base

technique (WALSH, 1995) and reduction of the blind spot using signal processing techniques (KWAK et al., 2008). Another approach is applying the method from both perspectives, in other words, applying the pulse and monitoring the reflections from port one and also from port two, enabling the reading of both ends of the channel under test once the blind spot of the first perspective will be the end of the line on the second one.

Another problem related to the TDR method is given by the attenuation that the pulse will suffer while traveling along the line, being a function of the distance traveled. Losses in the bulk insulation and propagation through the resistance of the channel components induce energy loss of an incident pulse (HERNANDEZ-MEJIA, 2016). TDR pulses with narrow width, composed by high frequency components, suffer higher attenuation than the wider ones, with low frequency components. Attenuation increases with frequency and for long channels the pulses can attenuate until reach the noise background level, hiding the reflections information. In addition to the attenuation, the TDR pulse suffers also dispersion and distortion. Different frequency components travel along the channel at different speeds, causing a phase shift of each frequency component of the TDR pulse, being a function of the distance traveled by the pulse and its frequency components profile (HERNANDEZ-MEJIA, 2016). Both distortions attenuation and dispersion can occur simultaneously, affecting the accuracy of locating impedance mismatches along the channel.

There is a tradeoff when specifying the pulse width and amplitude to apply the TDR method. Both affect the TDR resolution, in other words the ability to identify all those impedance mismatches along the channel under test. Having a good amplitude resolution means that even small changes in the reflection coefficient can be identified over the TDR trace, in a way that all the reflection coefficients of the channel will be represented by an amplitude higher than the background noise. So, the amplitude resolution is directly linked to the distance that the incident pulse or reflection is able to travel without reaching the noise level amplitude. In other hand, the time resolution is referred to the ability to distinguish two impedance mismatches locations closely spaced. The wider the pulse, the harder to recognize them. The tradeoff between the amplitude and time resolution is all based on attenuation and dispersion. Improving time resolution by using a narrower pulse may compromise the amplitude resolution, as well as improving the amplitude resolution using wider pulse may compromise the time resolution. Therefore, there is an optimal point when choosing amplitude and width of the TDR pulse.

In addition to the reflection coefficients along the line, the reflected wave also reveals the nature of mismatches based on the shape of each reflection. Figure 5 illustrates possible shapes to achieve over a TDR trace, either using a step or an impulse as incident wave:

Element	Step response	Impulse response
Open circuit	 Unity reflection	 Unity reflection
Short circuit	 Unity reflection -180°	 Unity reflection -180°
$R > Z_0$	 Positive level shift	 Positive peak
$R < Z_0$	 Negative level shift	 Negative peak
Inductor	 Positive peak	 Positive then negative peaks
Capacitor	 Negative peak	 Negative then positive peaks

**Figure 5 - Different shapes of reflections and their meanings** (AGILENT TECHNOLOGIES, 2012).

The far end location of a given channel under test can be easily identified by performing the TDR using open circuit and short circuit terminations. Using either an impulse or step as an incident wave the shape of the wave reflected in open termination is a positive unity reflection, whereas in short termination is a negative unity reflection. Once the difference between those two traces is only the termination used, the end of the line location is given by the time at which the traces differentiate between them by the positive unity reflection and the negative one.

Considering the impulse response, increasing on impedance along the line can be identified over the TDR trace as positive peaks, while decreasing on impedance as

negative peaks. Inductance characteristics are revealed by positive followed by negative peaks, while locations with capacitance characteristics the contrary.

As described, time domain reflectometry method requires ideal open and short circuit terminations, which are difficult to achieve over a broadband frequency range. Moreover, open circuit terminations cause stray capacitance due to electric field fringing at high frequencies, while short circuit terminations introduce additional inductance (PAPAZYAN et al., 2004).

### 2.2.2 Scattering Parameters

Scattering parameters are widely used for characterizing n-port networks. These parameters relate travelling waves to the network behavior, rather than voltages and currents. The waves scattered or reflected from the network are related to those waves incident upon the network (AGILENT TECHNOLOGIES, 2006). From them it is possible to extract the characteristic impedance, propagation constant and the distributed parameters (resistance, inductance, conductance and capacitance) as well of the line (PAPAZYAN et al., 2004).

The scattering matrix  $S$  represents the relationship between the normalized incident voltage waves  $[V^+]$  and the normalized reflected ones  $[V^-]$  as (2.54):

$$[V^-] = [S][V^+] , \quad (2.54)$$

which can be detailed as (2.55):

$$\begin{bmatrix} V_1^- \\ V_2^- \\ \vdots \\ V_i^- \end{bmatrix} = \begin{bmatrix} S_{11} & S_{12} & \dots & S_{1j} \\ S_{21} & S_{22} & \dots & S_{2j} \\ \vdots & \vdots & \ddots & \vdots \\ S_{ij} & S_{2j} & \dots & S_{ij} \end{bmatrix} \cdot \begin{bmatrix} V_1^+ \\ V_2^+ \\ \vdots \\ V_j^+ \end{bmatrix} . \quad (2.55)$$

Each element of the scattering matrix describes the electrical behavior related to two specific ports of the network under analysis. The parameter  $S_{ij}$  relates the reflected wave from port  $i$  to the incident wave from port  $j$  as (2.56):

$$S_{ij} = \frac{V_i^-}{V_j^+} . \quad (2.56)$$

Rather than short or open circuit terminations as demanded in methods for characterizing based on the reflectometry principle, the extraction of the scattering parameters is made by terminating one or the other port with the normalizing impedance  $Z_0$  of the network analyzer equipment, which is normally 50  $\Omega$ . For a given

2-port network, there will exist four scattering parameters, and the topology for acquiring them is shown in Figure 6.

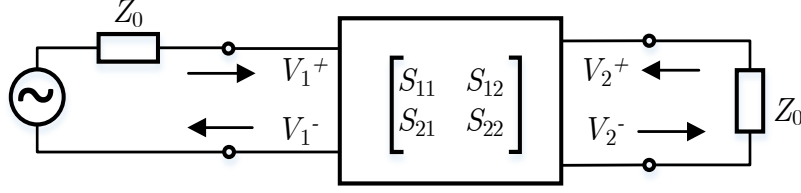


Figure 6 - Scattering parameters measurement topology for 2-port network.

And its  $S$  matrix is given by (2.57):

$$\begin{bmatrix} V_2^- \\ V_1^- \end{bmatrix} = \begin{bmatrix} S_{11} & S_{12} \\ S_{21} & S_{22} \end{bmatrix} \begin{bmatrix} V_2^+ \\ V_1^+ \end{bmatrix}, \quad (2.57)$$

being  $S_{11}$  the input reflection coefficient with matched output,  $S_{21}$  the forward transmission coefficient with matched output,  $S_{22}$  the output reflection coefficient with matched input, and  $S_{12}$  the reverse transmission coefficient with matched input (AGILENT TECHNOLOGIES, 2006). Therefore, the parameters  $S_{11}$  and  $S_{22}$  are related with how matched is the network referenced to  $Z_0$ , whereas  $S_{12}$  and  $S_{21}$  are related to how the network attenuates or amplifies an input signal.

When a network has the same transmission and reflection characteristics from port one to port two in comparison to the contrary perspective, it is designated as a reciprocal network (AGILENT TECHNOLOGIES, 2006). The S-parameter matrix of this kind of network is equal to its transpose, implying  $S_{11}=S_{22}$  and  $S_{12}=S_{21}$ .

The scattering parameters can also be written in terms of transmission line wave propagation characteristics as (2.58) (PAPAZYAN et al., 2004)

$$[S] = \frac{1}{D_s} \begin{bmatrix} (Z_c^2 - Z_0^2) \sinh \gamma l & 2Z_c Z_0 \\ 2Z_c Z_0 & (Z_c^2 - Z_0^2) \sinh \gamma l \end{bmatrix}, \quad (2.58)$$

being  $D_s = 2Z_c Z_0 \cosh \gamma l + (Z_c^2 + Z_0^2) \sinh \gamma l$  and  $l$  the line length.

Assuming that the line is reciprocal ( $S_{11} \equiv S_{22}$  and  $S_{21} \equiv S_{12}$ ), the propagation constant  $\gamma$  can be derived from (2.58), written in function of these parameters as (2.59)

$$\gamma(\omega) = \frac{1}{l} \cosh^{-1} \left( \frac{1 - S_{11}^2 + S_{21}^2}{2S_{21}} \right), \quad (2.59)$$

as well the characteristic impedance  $Z_c$  as (2.60)

$$Z_c(\omega) = Z_0 \sqrt{\frac{(1 + S_{11})^2 - S_{21}^2}{(1 - S_{11})^2 - S_{21}^2}}. \quad (2.60)$$

The distributed parameters can be deduced from the definition of propagation constant (2.12) and characteristic impedance (2.21) as (2.61)

$$\begin{aligned} R(\omega) &= \operatorname{Re}\{\gamma Z_C\} \\ L(\omega) &= \operatorname{Im}\{\gamma Z_C\} / \omega \\ G(\omega) &= \operatorname{Re}\{\gamma / Z_C\} \\ C(\omega) &= \operatorname{Im}\{\gamma / Z_C\} / \omega \end{aligned} \quad (2.61)$$

### 2.2.2.1 Scattering parameters in time domain

Scattering parameters can be converted to time domain to provide an impedance profile and impulse response of the line under test. As seen in section 2.2.1, reflectometry based methods enable to find physically faults and impedance mismatches along the line, which is also possible to achieve from the analysis of the parameter  $S_{11}$  converted to time domain. Whereas, time domain transmission analysis give the impulse response of the line, equivalent to the integral of the parameter  $S_{21}$  converted to time domain. The conversion is achieved by mathematical tools that enable the change on the analysis scenario from frequency to time domain, and vice-versa. One conversion method usually performed by a number of commercial Network Analyzers is the Inverse Chirp Z Transform, but before to explain it, one must to define the direct Chirp Z Transform. Proposed by Lawrence Rabiner in 1969, the Chirp Z Transform consists in an algorithm that evaluates the Z transform of a sequence of  $N$  samples at  $M$  points in the Z plane, standing either right on circular or spiral contours beginning at any arbitrary point (RABINER; SCHAFER; RADER, 1969). The Chirp Z Transform of sequence  $\{x(n)\}$  with  $0 \leq n < N-1$  is defined as (2.62)

$$X(k) = \sum_{n=0}^{N-1} x[n] \left( A_{CZT} W^{-k} \right)^{-n}, \quad (2.62)$$

being  $X(k)$  the resulting  $M$  points sequence defined in  $0 \leq k < M-1$  and,  $A_{CZT}$  and  $W$  arbitrary complex numbers defined by (2.63) and (2.64)

$$A_{CZT} = A_0 e^{j2\pi\theta_0}, \quad (2.63)$$

$$W = W_0 e^{-j2\pi\varphi_0}. \quad (2.64)$$

$A_{CZT}$  is the starting point for the sweeping in Z plane, and  $W$  defines how the contour spirals over the plane.  $A_0$  and  $\theta_0$  are the starting radius and angle respectively, and  $\varphi_0$  the angle step size.  $W_0$  sets the rate at which the contour spirals in (greater than 1) or out (less than 1) from a circle of radius  $A_0$ . Therefore, the contour at which



the Chirp Z transform is defined in the Z plane, shown in Figure 7, is set by the term  $A_{CZT} W^k$ .

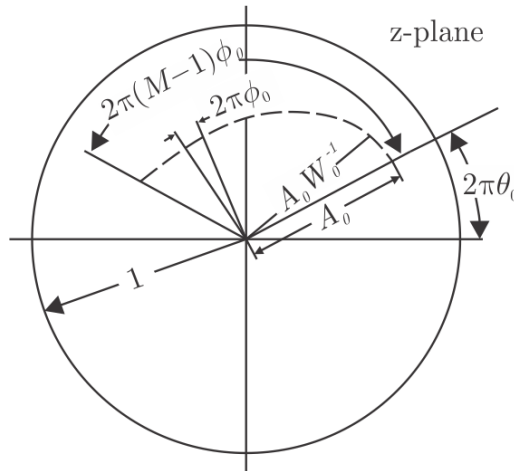


**Figure 7 - Chirp Z Transform: spiral contour in the Z plane. Adapted from (RABINER; SCHAFER; RADER, 1969).**

From this definition, Discrete Fourier Transform can be interpreted as a specific case of the Chirp Z Transform for being restricted to the unit circle in the z plane.

Among the advantages provided by the Chirp Z Transform, one can list: the output sampling can be different from the input one ( $N \neq M$  or  $N = M$ ); both  $N$  and  $M$  can be prime numbers; arbitrary frequency resolution given by arbitrary angular spacing along the contour; random starting point of analysis in the Z plane, enabling narrow-band analysis.

The analysis of the scattering parameters in time domain requires the solution for the inverse problem, performed by the Inverse Chirp Z Transform (*ICZT*). Mersereau has developed an algorithm to calculate the Inverse Chirp Z Transform through the relation  $ICZT(X(k)) = A_{CZT}^{-n} CZT(1, W^{-1}, C_k X(k), N)$ , with  $C_k$  a calculated coefficients array (MERSEREAU, 1974). Although, even the author mentions that the number of problems to which the proposed algorithm might be applied is extremely sensitive to quantization errors. Frickey has proposed that the inverse transform can be accomplished by  $ICZT(X(k)) = [CZT(X(k)^*)]^*$ , but the performance is only guaranteed for the *CZT* operating at or inside the unit circle in the Z plane (FRICKEY, 1994). Another approach is presented by Yague et al., following a direct method as (2.65):

$$x(t_1 + n\delta t) = \frac{1}{M} \sum_{k=0}^{M-1} X(k) e^{j2\pi(f_1 + k\delta f)(t_1 + n\delta t)}, \quad n = 0, 1, \dots, N-1 \quad (2.65)$$

being the data in time domain denoted by  $x(t_1+n\delta t)$ , start frequency and time by  $f_1$  and  $t_1$  respectively, the step frequency and time by  $\delta f$  and  $\delta t$  respectively (DE PORRATA-DORIA I YAGUE; IBARS; MARTINEZ, 1998).

Although the arbitrariness of *CZT* in choosing the number of input and output samples is considered an advantage, it can also bring matters to the inverse problem scenario. The difference between the sampling set in frequency and in time can render unstable inversion due to ill-posedness of the problem.

### 2.2.3 *ABCD* Matrix

The *ABCD* Matrix (or Transmission Matrix) is another method to characterize a two-port network, which defines four variables that relate total voltage and current in each port as (2.66):

$$\begin{aligned} V_1 &= A V_2 + B I_2 \\ I_1 &= C_{ABCD} V_2 + D I_2 \end{aligned} \quad (2.66)$$

Rewriting (2.66) in matrix form leads to (2.67):

$$\begin{bmatrix} V_1 \\ I_1 \end{bmatrix} = \begin{bmatrix} A & B \\ C_{ABCD} & D \end{bmatrix} \begin{bmatrix} V_2 \\ I_2 \end{bmatrix} \quad (2.67)$$

Figure 8 shows a diagram for the *ABCD* Matrix representation of a two-port network. It is important to exalt that for this model the current  $I_2$  flows from port 2, instead of into port 2 as used in scattering parameters model. The sign convention when dealing with *ABCD* matrices is different so that in a cascade network  $I_2$  will be the same current that flows into the adjacent network (POZAR, 2005).

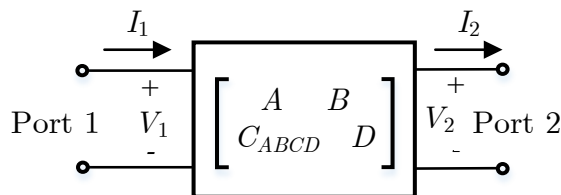


Figure 8 – Two-port network - *ABCD* matrix representation.

The main convenience on using this kind of representation is that the *ABCD* matrix of a cascaded connection of any number of two-port networks can be achieved by multiplying the *ABCD* matrices of each one of them. Considering a cascaded connection composed by two two-port networks, as shown in Figure 9.

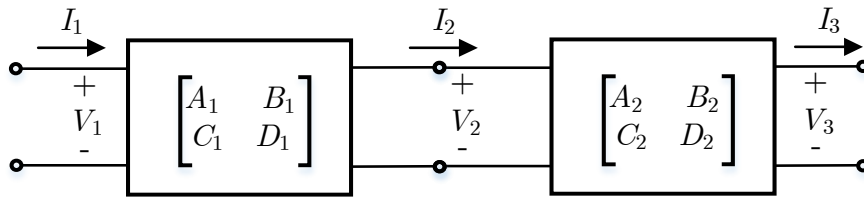


Figure 9 - Two-port networks in cascaded connection.

The  $ABCD$  matrix for the individuals two-ports is given by (2.68) and (2.69):

$$\begin{bmatrix} V_1 \\ I_1 \end{bmatrix} = \begin{bmatrix} A_1 & B_1 \\ C_1 & D_1 \end{bmatrix} \begin{bmatrix} V_2 \\ I_2 \end{bmatrix}, \quad (2.68)$$

$$\begin{bmatrix} V_2 \\ I_2 \end{bmatrix} = \begin{bmatrix} A_2 & B_2 \\ C_2 & D_2 \end{bmatrix} \begin{bmatrix} V_3 \\ I_3 \end{bmatrix}. \quad (2.69)$$

Substituting (2.69) in (2.68) leads to (2.70):

$$\begin{bmatrix} V_1 \\ I_1 \end{bmatrix} = \begin{bmatrix} A_1 & B_1 \\ C_1 & D_1 \end{bmatrix} \begin{bmatrix} A_2 & B_2 \\ C_2 & D_2 \end{bmatrix} \begin{bmatrix} V_3 \\ I_3 \end{bmatrix}, \quad (2.70)$$

which is equal to the product of the individual  $ABCD$  matrices. One must exalt that the order of multiplication of the matrices must be the same as the networks are arranged.

The  $ABCD$  parameters can also be related to the secondary parameters of a reciprocal transmission line characteristic impedance and propagation constant (LAMPE; TONELLO; SWART, 2016), defined by (2.71):

$$\begin{aligned} A &= D = \cosh(\gamma d) \\ B &= Z_c \sinh(\gamma d) \\ C_{ABCD} &= Z_c^{-1} \sinh(\gamma d) = BZ_c^{-2} \end{aligned}, \quad (2.71)$$

with the total line length denoted by  $d$ . Rewriting the  $ABCD$  parameters in matrix notation one obtains (2.72):

$$\begin{bmatrix} A & B \\ C_{ABCD} & D \end{bmatrix} = \begin{bmatrix} \cosh(\gamma d) & Z_c \sinh(\gamma d) \\ Z_c^{-1} \sinh(\gamma d) & \cosh(\gamma d) \end{bmatrix}. \quad (2.72)$$

Then one can relate those parameters to the input impedance of a set composed by a given transmission line terminated in a load impedance  $Z_L$  as (2.73):

$$Z_{in} = Z_c \frac{Z_L \cosh \gamma d + Z_c \sinh \gamma d}{Z_c \cosh \gamma d + Z_L \sinh \gamma d} = \frac{AZ_L + B}{C_{ABCD}Z_L + D}. \quad (2.73)$$

Now considering the channel plus load set connected to a source with impedance  $Z_s$ . Its transfer function can be written in function of those  $ABCD$  parameters as (2.74) (FRANCIS; TITUS, 2011):

$$H(f) = \frac{Z_L}{AZ_L + B + C_{ABCD}Z_SZ_L + DZ_S} . \quad (2.74)$$

### 2.2.4 Impedance Spectroscopy

The impedance spectroscopy method consists in measuring impedance of a particular material under test over a given frequency spectrum, which enables the analysis of the changes of electrical properties in each frequency. The principle of this method is relating the input impedance measured at each frequency to the characteristic impedance and to the propagation constant of the line under test. Considering a transmission line terminated in short circuit ( $Z_L=0$ ), the input impedance presented in equation (2.30) becomes (2.75):

$$Z_{short} = Z_c \tanh(\gamma d) , \quad (2.75)$$

with the total line length denoted by  $d$ . Using the same logic, but now considering an open circuit as termination ( $Z_L \rightarrow \infty$ ) the input impedance will be (2.76):

$$Z_{open} = Z_c / \tanh(\gamma d) . \quad (2.76)$$

Through the relations between the definition of  $\gamma$  (2.12), impedance for short circuit as load (2.75) and impedance for open load (2.76), one can obtain expressions for the characteristic impedance (2.77) and propagation constant (2.78) (QINGHAI SHI; TROLTZSCH; KANOUN, 2011):

$$Z_c = \sqrt{Z_{short} Z_{open}} , \quad (2.77)$$

$$\gamma = \sqrt{\frac{Z_{short}}{Z_{open}}} . \quad (2.78)$$

Then, the distributed parameters can be extracted following the same relations presented in equations (2.61).

### 2.2.5 Shannon-Hartley Theorem

Shannon-Hartley theorem states that the theoretical tightest upper bound on the information rate of data that can be performed at a communication system operating at a bandwidth  $BW$  (Hz) using an average signal power  $S$  (W) through a channel subject to additive white Gaussian noise power level  $N$  (W) is given by (2.79) (SHANNON, 1948):

$$C_{\max} = BW \log_2 \left( 1 + \frac{S}{N} \right), \quad (2.79)$$

being the channel capacity represented by  $C_{\max}$  (bps), and signal-to-noise ratio (SNR) designed by the relation between the communication signal to the noise at the receiver, as a linear power ratio.

A Gaussian noise is defined as a filtered thermal noise, with power spectrum  $N(f)$ . For a channel perturbed by any Gaussian noise, channel capacity can be written as frequency dependent function, dividing the band into a large number of small bands, with  $N(f)$  approximately constant in each. The total capacity for a given distribution  $S(f)$  can be written as (2.80) (SHANNON, 1949):

$$C_{\max} = \int_0^{BW} \log_2 \left( 1 + \frac{S(f)}{N(f)} \right) df. \quad (2.80)$$

### 2.2.6 LTI Channel Model

A Linear Time Invariant channel is defined as the channel which has constant frequency response  $H(f)$  over time. In other words, the electrical characteristics of the channel do not vary over time. For instance, wireless channels are commonly treated as time variant since the electrical properties of the medium cannot be assumed constant, while the wired ones are treated as time invariant since the immunity to external elements.

A channel is classified as a block fading frequency response channel when it is assumed that the response can be divided into subchannels of bandwidth  $BW$  with constant  $H(f) = H_j$  (GOLDSMITH, 2005), as depicted in Figure 10.

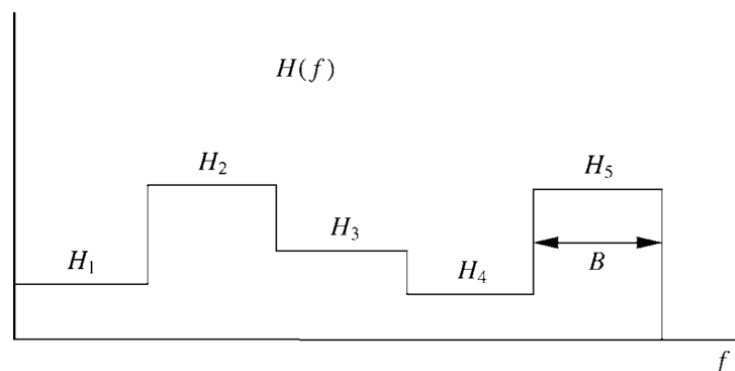


**Figure 10** – Frequency selective fading channel (GOLDSMITH, 2005).

This channel is composed then by a set of AWGN channels in parallel with SNR  $|H_j|^2 P_j / N_0 BW$  on the  $j$ th channel, with power allocated  $P_j$  to the  $j$ th channel. So the total capacity of the channel is the sum of rates on each subchannel as (2.81):

$$C_{\max} = \sum_{\max P_j: \sum_j P_j \leq P} BW \log_2 \left( 1 + \frac{|H_j|^2 P_j}{N_0 BW} \right). \quad (2.81)$$

### 2.3 ORTHOGONAL FREQUENCY DIVISION MULTIPLEXING

Orthogonal Frequency Division Multiplexing (OFDM) is a promising multicarrier modulation technique for PLC applications, presenting high spectral efficiency and properties that mitigate the harsh characteristics of power line channels (KOTCHASARN, 2017). Its principle consists in splitting a high rate data stream into a number of lower rate streams and transmit them simultaneously over a number of orthogonal subcarriers, which ensures the non-interference between them. The orthogonality property can be lost due to multipath or non-stationary behavior of the channel, causing intersymbol interference (ISI). The phenomenon drastically degrades the received signal, being one of the major obstacles that high data rate systems must overcome (RAHMAN; MAJUMDER, 2014). However, ISI can be avoided completely or can be reduced at least considerably by a proper choice of OFDM system parameters (ROHLING, 2011).

Essentially the transmission process involves assembling the input information into  $N$  blocks of complex numbers, one for each sub-channel. Then, an Inverse Fast Fourier Transform (IFFT) is performed on each block, resulting in  $N$  separate QAM signal with spectrum shaped as *sinc* function, with nulls at the center of the other sub-carriers (BAHAI; SALTZBERG; ERGEN, 2004). The resultant signal is transmitted serially over the channel. At the receiver, the information is recovered by performing an FFT on the received block of signal samples. A simple block diagram of an OFDM system is presented in Figure 11.

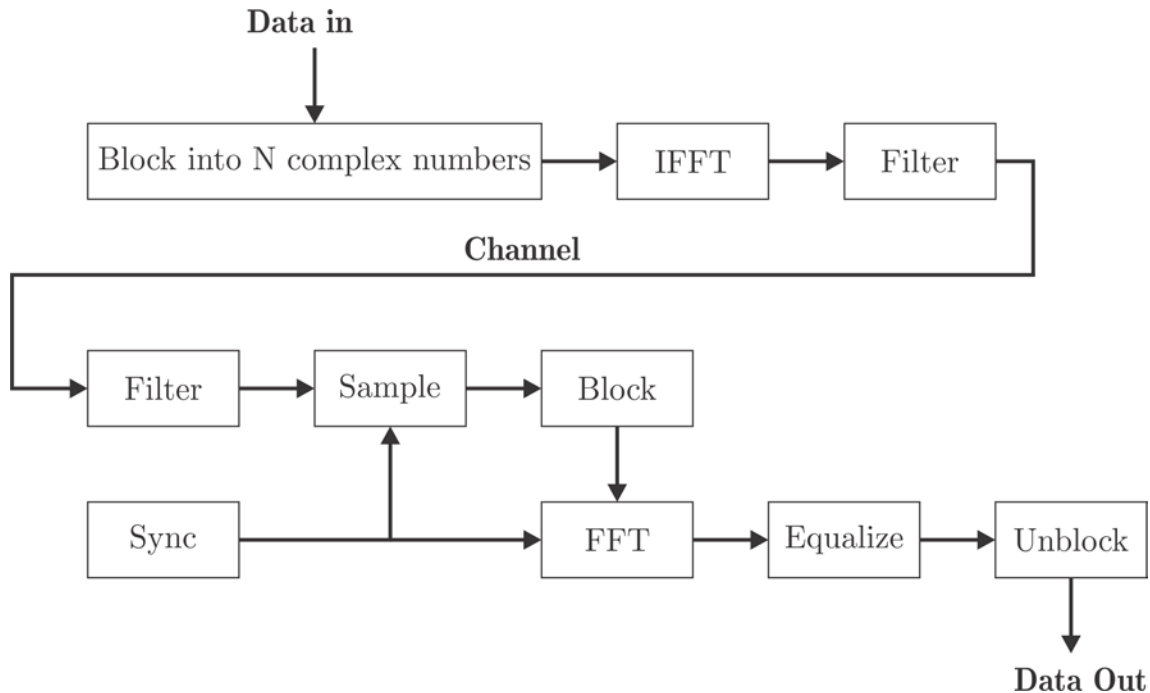


**Figure 11 - Block diagram of basic OFDM system. Adapted from (BAHAI; SALTZBERG; ERGEN, 2004).**

To avoid overlap of consecutive transmitted blocks, a short cyclic prefix on the transmit signal is used, acting as a buffer between blocks (LIN; PHOONG; VAIDYANATHAN, 2011). This feature allows perfect distortionless data recovery at the transmitter, even for dispersive channels. However, prefixing leads to an increasing on the use of bandwidth.

OFDM characteristics enable transmission over extremely hostile channel at a comparable low complexity with high data rates, and because of them this modulation technique has been adopted in important wireless communication systems such as Digital Audio Broadcasting (DAB), Digital Video Broadcasting (DVB), Wireless Local Area Network (WLAN), Wireless Metropolitan Area Network (WMAN), and Multi Band – OFDM Ultra Wide Band Besides. OFDM is also employed in wired applications such as Asymmetric Digital Subscriber Line (ADSL) and Power Line Communication (PLC) (RAHMAN; MAJUMDER, 2014).

### 2.3.1 Power Line Communication

Power Line Communication (PLC) is the name given to the technology with the purpose of implementing data transmission over existed structures already used on energy distribution. The transmission occurs through modulation in high frequency

signals, going from hundreds of Hertz to hundreds of Mega Hertz (LAMPE; TONELLO; SWART, 2016). Its nature is intrinsic to the fact that the physical medium used for transmission is inserted in harsh environments considering electromagnetic interference, as well as channel parameters such as nominal noise, impedance and attenuation.

The PLC technology uses DFT-based transceivers. This is related to the modulation technique employed. For wired DSL (Digital Subscriber Line) applications it is designated as a DMT (Discrete Multitone) based system, whereas for wireless local area networks and broadcasting applications as OFDM (Orthogonal Frequency Division Multiplexing) based system (LIN; PHOONG; VAIDYANATHAN, 2011).

In DMT based systems, signals are transmitted over copper lines, which implies that the channel characteristics do not vary constantly. This feature enables power allocation over the subcarriers considering the channel state information evaluated by the system, allowing the exploitation of the disparity among the subchannel noise variances for a bit rate maximization (LIN; PHOONG; VAIDYANATHAN, 2011). In OFDM systems, there is no such constancy on channel behavior, so the transceiver operates independently and, therefore, with no power allocation. That is the reason why OFDM appears as a very useful modulation technique for broadcasting applications, where there are many receivers operating at the same transmission paths.

### 2.3.1.1 HomePlug AV2

The reuse of existing wires to deploy wide band services has attracting industry and research communities to dedicate attention to in-home power line communication. In 2001 HomePlug Alliance, an industry-led organization, created a set of specifications within the scope of power line networking, first named HomePlug 1.01. Then, in 2005 it was released a second version under the name HomePlug AV (ALLIANCE; RESERVED, 2005). The AV acronym abbreviates “Audio,Video”, refereeing to its data streaming application. HomePlug AV provides 200 Mbps class power line networking capability through PHY (Physical layer) and MAC (Media Access Control) technologies (YONGE et al., 2013). PHY layer operates in the frequency range of 2-28 MHz, using windowed OFDM and a powerful Turbo Convolutional Code (TCC) that provides robust performance within 0.5 dB of Shannon’s limit. OFDM operates into 917 carriers with a flexible guard interval. 1024 QAM (Quadrature Amplitude



Modulation) and Binary Phase Shift Keying (BPSK) techniques are employed adaptively to each carrier based on the channel characteristic (ALLIANCE; RESERVED, 2005). On the MAC layer HomePlug AV employs Quality of Service (QoS) connection oriented, contention-free service on a periodic Time Division Multiple Access (TDMA) allocation, and a connectionless, prioritized contention-based service on a Carrier Sense Multiple Access / Collision Avoidance (CSMA/CA) allocation. MAC stream is divided into 512 octet segments, encrypted and encapsulated into serialized PHY Blocks (PBs), and packed as MAC Protocol Data Units (MPDUs) to the PHY unit. The final PHY Protocol Data Unit (PPDU) is generated to be transmitted onto the power line (ALLIANCE; RESERVED, 2005).

In the year of 2013 Home Alliance group released the HomePlug AV2 Technology (ALLIANCE HPGP, 2013). The architecture upgrade provides two to five times the performance of HomePlug AV, matching requirements to support the throughput and coverage needed for next-generation multimedia applications. There is an additional frequency spectrum of 30 MHz to 86 MHz beyond the bandwidth used for HomePlug AV, improving peak data rates and performance at all. HomePlug AV2 also incorporates Multiple-Input Multiple-Output (MIMO) capabilities with beamforming, which enables transmission on any two-wire pairs within three-wire configurations (line, neutral and ground), whereas HomePlug AV only allows transmission through line-neutral pair. In cases where there is no third wire available required to operate MIMO, HomePlug AV2 automatically switches to standard operation Single-Input Single-Output (SISO). In MIMO architecture two independent transmitters and up to four receivers, combined with beamforming maximize the performance on the independent streams (ALLIANCE HPGP, 2013). Besides, HomePlug AV2 provides lower latency and increases network efficiency through the incorporation of a high efficiency PPDU structure, with a lower packet overhead; efficient notching up to 20 % gain due to sharper PSD notches against fixed and relatively conservative windowed OFDM mechanism performed in HomePlug AV; PHY improvements like higher-order modulation (4096 QAM), higher code rates and smaller guard intervals; and power save mode for better energy efficiency. Despite of the 4096 subcarriers over 100 MHz on the HomePlug AV2 OFDM parameters specification, only 3455 carriers are supported for communication (1.8 to 86.13 MHz). The subcarrier spacing of 24.414 kHz was defined in the HomePlug AV and is maintained in AV2 for interoperability (YONGE et al., 2013).

### 3 METHODOLOGY

Aiming to explore the means to characterize a channel, two different experimental sets are proposed. The first one aims to investigate the influence of length over channel capacity, obtained from scattering parameters following the Shannon Hartley's theorem. The capacities are compared to real performance of a communication system running over the cables as channel. The second set investigates the electrical behavior of a channel at all, from time domain measurements analysis to frequency domain measurements analysis.

Both experimental sets exploit frequency analysis bands up to 4 GHz, covering the following bands defined by the International Telecommunications Union (ITU): medium frequency (MF: 300 kHz to 3 MHz), high frequency (HF: 3 MHz to 30 MHz), very high frequency (VHF: 30 MHz to 300 MHz), ultra high frequency (UHF: 300 MHz to 3 GHz) and a small part of super high frequency (SHF: 3 GHz to 30 GHz).

#### 3.1 INFLUENCE OF THE LENGTH OVER THE CHANNEL CAPACITY SET

Two different kinds of cables were selected to be characterized in a way to obtain their capacities in function of length and noise level. In addition, the performance of a communication system is verified using PLC devices running over those cables in different lengths as the channel. The idea is comparing the capacities in function of noise level and length curves to the performance obtained for each length set.

The selected cables are an unshielded twisted pair CAT5e and a flexible stranded two-wire copper 1.5 mm<sup>2</sup> pair, both starting with 100 meters as initial length, subsequently decreasing 10 meters in length at each round, until reach only 10 meters. The experiment consists in extracting the scattering parameters of each cable in each length set defined. From them it is achieved the frequency response for each length. Proceeding to the calculus of the channel capacity, curves are fitted from the response of each length case, considering the following channel response model (3.1) (EZZINE et al., 2017):

$$H(f) = e^{-(a_0 + a_1 f^{k_f})d} e^{-j2\pi f\tau} \quad . \quad (3.1)$$

The first term composed by an exponential of order  $-(a_0 + a_1 f^{k_f})d$  denotes the overall attenuation. The second one of order  $-j 2\pi f\tau$  is the delay of the wave, being  $\tau$  the

propagation delay. This model is similar to the one presented in section 2.1.5 as (2.48). The attenuation constant  $\alpha$  here is expressed as a sum of two parameters:  $a_0$ , the dependency of attenuation with the length  $d$ , and  $a_1$  the frequency and length dependent parameter. The phase constant  $\beta$  here is denoted by  $2\pi f\tau$ , with distance intrinsic to the propagation delay  $\tau$ .

Since the channel response corresponds to the norm of (3.1), the model is simplified as (3.2):

$$|H(f)| = e^{-(a_0 + a_1 f^k) d} . \quad (3.2)$$

Frequency  $f$  and length  $d$  are known. The parameters  $a_0$ ,  $a_1$  and  $k_f$  are calculated for each length set. Then new frequency response functions are defined from the fitted curves, but now only at the bandwidth from 1.8 MHz to round 86.13 MHz, with 3455 subcarriers equally spaced in 24.414 kHz. These are the parameters for bandwidth specified in HomePlug AV2 specifications, the PLC running technology. The response at this bandwidth defines the signal level for each length. Then, the channel capacity is calculated for each length following the Shannon-Hartley theorem. The signal to noise ratio is obtained by the difference between the signal level (obtained from the frequency response) and the noise levels of 20 dB, 30 dB and 40 dB.

The cables were selected in a way to analyze their electrical behavior considering two distinct constructive and electrical characteristics sets. The UTP CAT5e is a typical example of a cable for data communication purpose, whereas the flexible two-wire copper 1.5 mm<sup>2</sup> cable is typically found in residential and industrial plants, first designated for energy distribution. Their use on communication purpose has become attractive on PLC applications through existing copper structures. Figure 12 illustrates the two cables selected for analysis.



**Figure 12 –Cables selected for analysis: CAT5e UTP line (a) and flexible stranded two-wire copper 1.5 mm<sup>2</sup> (b).**

The scattering parameters of the cables were acquired using a Vector Network Analyzer ENA Series E5071C Agilent Technologies<sup>®</sup>, following the parameters set defined as: 200 kHz for step frequency, 20001 points, start frequency in 400 kHz and stop frequency in 4.0004 GHz. Full two-port calibration was done using the calibration kit 85052 B 3.5 mm Agilent Technologies<sup>®</sup>, where all four scattering parameters are fully corrected based on the SOLT calibration (short – open – load – through). The scattering parameters were extracted and compiled into a s2p touchstone file for each length set acquired. These data in frequency domain are processed in an algorithm developed in MATLAB<sup>®</sup>, where in first place the secondary parameters characteristic impedance and propagation constant are calculated. From them the frequency response is achieved, so the analysis continues as already described.

The PLC devices used are an AV1000 2-port kit commercially distributed by TP-Link<sup>®</sup> (TL-PA7020). The communication system used on the analysis of the performance of the channel is a server-client application developed in C++ language and runs over a TCP/IP protocol.

### 3.2 CHANNEL ANALYSIS THROUGH TIME DOMAIN AND FREQUENCY DOMAIN DATA

Figure 13 presents the characteristics of the channel chosen to be characterized through time and frequency domain. The channel is composed by four sections of coaxial cables with different characteristic impedance and length, totalizing about 56.19 meters long.

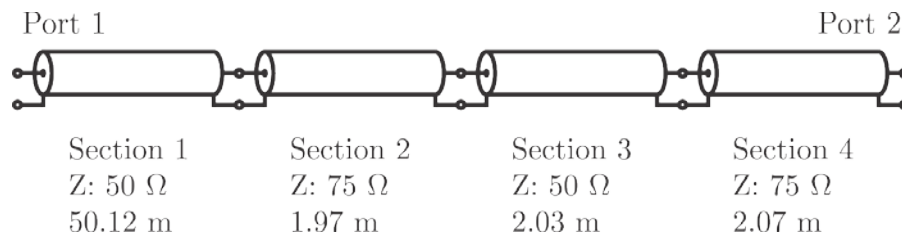


**Figure 13 - Channel set chosen to be characterized in time and frequency domain.**

The characteristic impedance and length of each section are respectively: 50 Ω 50.12 m, 75 Ω 1.97 m, 50 Ω 2.03 m, and 75 Ω 2.07 m. The set was chosen in a way that the transitions between the sections could be evident in traces through time domain profiles. As a matter of designation, section 1's end is defined as port 1, whereas section 4's end as port 2.

### 3.2.1 Frequency Domain Data Acquisition and Analysis

The scattering parameters of the channel are acquired also using the Vector Network Analyzer ENA Series E5071C Agilent Technologies<sup>®</sup>. These data in frequency domain are processed in an algorithm developed in MATLAB<sup>®</sup>, where in first place the secondary parameters (characteristic impedance and propagation constant) are calculated, and then the primary ones: distributed resistance, inductance, conductance and capacitance. Also from the secondary ones it is possible to achieve the channel frequency response, which added to a noise model leads to the Shannon channel capacity. This completes the whole set of analysis in frequency domain. On other hand, the analysis of the channel in time domain is made by the conversion of the frequency domain scattering parameters using the Inverse Chirp Z Transform. Results are the impulse response, given by the analysis of the parameter  $S_{21}$  in time domain, and the impedance profile of the channel, given by the parameter  $S_{11}$  in time domain. In addition, it is proposed a different approach for the conversion to time domain, leaded by a sparse solution of the problem, which it is detailed explained in the following subsection 3.2.1.1. Figure 14 illustrates the set of the proposed analysis of the channel.

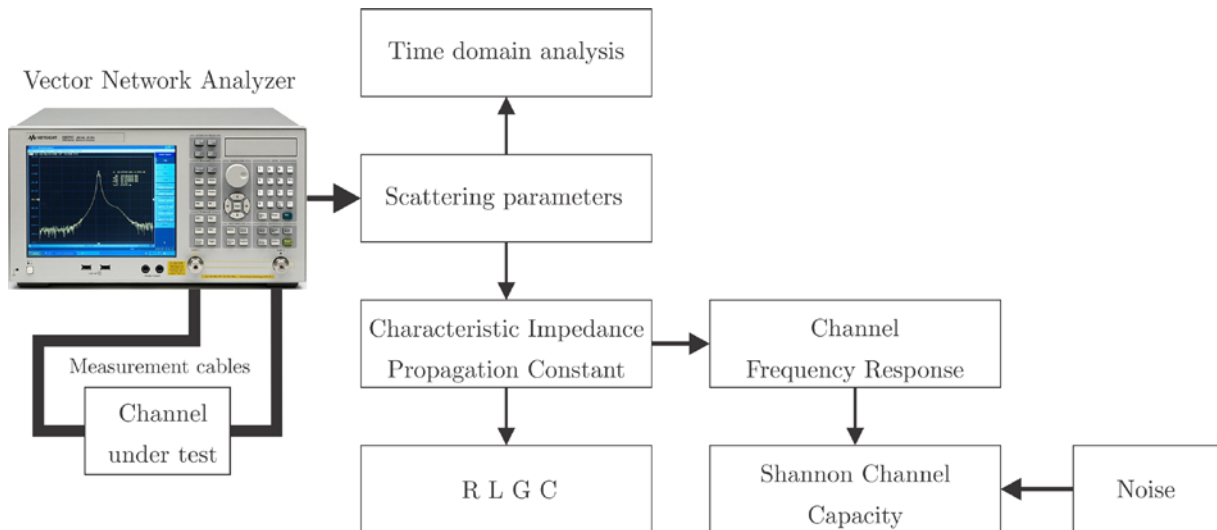


**Figure 14 - Block diagram for the channel analysis proposed.**

Before starting the measurements, one must select the frequency parameters set. Essentially, this selection will define more than just resolution and span for the analysis in frequency domain, but also the time domain analysis configurations. The maximum time for sampling is defined by the alias free range (ANRISTU, 2016) as (3.3)

$$t_{\max} = \frac{1}{2\delta f} . \quad (3.3)$$

Since the maximum length to be characterized is about 56 meters, round trip considering the propagation speed through the channel in 66 % of the speed of light is about 567 ns. This assumption is based on the fact that the dielectric insulation of the coaxial cables used is made of polyethylene (AGILENT TECHNOLOGIES, 2012) From (3.3) the step frequency  $\delta f$  for this analysis shall be nearly about to 881.8 kHz. So, this is the maximum step frequency required to cover the entire length of the channel under test. Bigger values than this will not be sufficient to characterize the round trip in time domain analysis. For a higher definition of the frequency response, the step frequency selected for the measurements was 200 kHz.

The resolution in time domain analysis is defined in meters by the frequency span  $\Delta F$  of the data acquired as (3.4)

$$Resolution = \frac{0.5 * c * V_{rel}}{\Delta F} , \quad (3.4)$$

being  $V_{rel}$  the relative speed of the signal on the channel. In this way, a resolution of 1 cm requires a frequency span of 9.9 GHz, 5 cm 1.98 GHz and 10 cm 990 MHz. As long as the maximum cable length is about 56 meters, and there is no need for a high resolution since it is not expected high variations in impedance along the component cables, the resolution is acceptable for smaller values than 10 cm. The frequency span selected for measurements is 4 GHz, which leads to a resolution of about 2.5 cm.

The parameters set is defined as 200 kHz for step frequency, 20001 points, start frequency in 400 kHz and stop frequency in 4.0004 GHz. Full two-port calibration was done using the calibration kit 85052 B 3.5 mm Agilent Technologies<sup>®</sup>, where all four scattering parameters are fully corrected based on the SOLT calibration (short – open – load – through). The scattering parameters were extracted and compiled into a s2p touchstone file. From this file, data in frequency domain were extracted and processed by an algorithm developed in MATLAB<sup>®</sup> that performs the whole analysis proposed, as already described.

### 3.2.1.1 Sparse Inverse Chirp-Z Transform for Time Domain Analysis

As presented in subsection 2.2.2.1, scattering parameters can be converted from frequency domain to time domain through the Inverse Chirp Z Transform. Casting the

Chirp Z Transform operation in a matrix format, the expression that implements (2.62) can be written as (3.5)

$$X = C_{CZT}x , \quad (3.5)$$

being  $C_{CZT}$  the CZT  $M \times N$  matrix. For  $M=N$ ,  $C_{CZT}$  implements a DFT and the inverse operation is given by  $C_{CZT}^*$  (hermitian) since  $C_{CZT}$  becomes unitary. Yet for the general CZT matrix, the inverse can not be  $C_{CZT}^*$  since some rows were modified, added or even discarded.  $C_{CZT}^*$  leads to the minimum norm solution (3.6)

$$x = C_{CZT}^* (C_{CZT} C_{CZT}^*)^{-1} X , \quad (3.6)$$

which does not have strong support.

It is proposed a sparse reconstruction instead, aiming to represent the signal, sparse in time, related to the reflections along the line. The reconstruction method proposed is based on an L2-L1 minimization problem, being L2 the data-fidelity term and L1 the sparse promoting term. The estimated solution  $x$  is given by the relation (3.7)

$$x = \arg \min \|C_{CZT}x - X\|_2^2 + \lambda_{CZT} \|x\|_1 , \quad (3.7)$$

where  $\lambda_{CZT}$  is the regularization parameter. The Fast Iterative Shrinkage-Thresholding Algorithm (FISTA) was chosen to solve (3.7), due to its simple implementation and fast convergence. FISTA is an efficient first-order method for minimizing a composite convex cost function (L2) with a convex non-smooth term (L1) (BECK; TEBoulLE, 2009a). The solution  $x$  will be a sparse signal representing the reflection coefficients on the line under test.

FISTA is a gradient based method derived from the first proposed ISTA (Iterative Shrinkage-Thresholding Algorithm) (BECK; TEBoulLE, 2009b). Considering the unconstrained minimization problem of a continuously differentiable function  $f: \mathbb{R}^n \rightarrow \mathbb{R}$  (3.8):

$$\min\{f(x) : x \in \mathbb{R}^n\} . \quad (3.8)$$

As a matter of designation,  $f$  denotes the composite convex cost function  $\|C_{CZT}x - X\|_2^2$  presented in (3.7). One of the simplest methods for solving (3.8) is the gradient method, which generates a sequence  $\{x_k\}$  as (3.9):

$$x_0 \in \mathbb{R}^n, x_k = x_{k-1} - t_k \nabla f(x_{k-1}) , \quad (3.9)$$

being  $t_k > 0$  a suitable stepsize. This gradient iteration can also be interpreted as a proximal regularization of the linearized function  $f$  at  $x_{k-1}$  (BECK; TEBoulLE, 2009b) as (3.10):

$$x_k = \arg \min \left\{ f(x_{k-1}) + \langle x - x_{k-1}, \nabla f(x_{k-1}) \rangle + \frac{1}{2t_k} \|x - x_{k-1}\|^2 \right\} . \quad (3.10)$$

Taking the same gradient deployment to the nonsmooth  $l_1$  regularized problem (3.11)

$$\min\{f(\mathbf{x}) + \lambda\|\mathbf{x}\|_1 : \mathbf{x} \in \mathbb{R}^n\} \quad (3.11)$$

leads to a new sequence (3.12):

$$\mathbf{x}_k = \arg \min \left\{ f(\mathbf{x}_{k-1}) + \langle \mathbf{x} - \mathbf{x}_{k-1}, \nabla f(\mathbf{x}_{k-1}) \rangle + \frac{1}{2t_k} \|\mathbf{x} - \mathbf{x}_{k-1}\|^2 + \lambda\|\mathbf{x}\|_1 \right\}. \quad (3.12)$$

This expression can be simplified by ignoring constant terms, leading to (3.13):

$$\mathbf{x}_k = \arg \min \left\{ \frac{1}{2t_k} \|\mathbf{x} - (\mathbf{x}_{k-1} - t_k \nabla f(\mathbf{x}_{k-1}))\|^2 + \lambda\|\mathbf{x}\|_1 \right\}. \quad (3.13)$$

The computation of  $\mathbf{x}_k$  can be reduced to solving a one-dimensional minimization problem for each of its components, because the norm  $l_1$  is separable. Thus, the final solution of  $\mathbf{x}_k$  can be given by a shrinkage operator  $\mathcal{T}_\alpha : \mathbb{R}^n \rightarrow \mathbb{R}^n$  as (3.14):

$$\mathbf{x}_k = \mathcal{T}_{\lambda t_k}(\mathbf{x}_{k-1} - t_k \nabla f(\mathbf{x}_{k-1})). \quad (3.14)$$

The logic presented above describes the development of ISTA solution. FISTA implements the same idea but through a different step logic based on an accelerated gradient-like method, which brings a faster convergence in the order of  $O(1/k_s^2)$  against  $O(1/k_s)$  performed by ISTA (BECK; TEBoulLE, 2009b).

The proposed method for the conversion of scattering parameters to time domain, named Sparse ICZT, was published in an article (WEBER et al., 2017) presented at the XXXV Brazilian Telecommunications and Signal Processing Symposium (SBrT), titled ‘‘Sparse Inverse Chirp-Z Transform of S-Parameter Measurements for Time Domain Analysis of Transmission Line’’.

### 3.2.2 Time Domain Data Acquisition and Analysis

The analysis of the channel under test in time domain consists in applying time domain reflectometry and transmissometry methods. Time domain reflectometry analysis consists in applying a known electrical pulse to the channel and verifying the reflected signal over time. The pulse is generated by a 330 MHz function generator (81160A Keysight®) and the reflected signal is read by an oscilloscope (MSOS104A Keysight®). Open, short and 50  $\Omega$  load are used as terminations connected at the far end of the channel, thus implying three steps for each pulse width configuration. Transmissometry analysis consists in applying a known pulse at the near end and



reading the response at the far end of the channel. In this case, there is no need for terminations neither the T connector. The scenario for the time domain profiles acquisition is depicted in Figure 15.

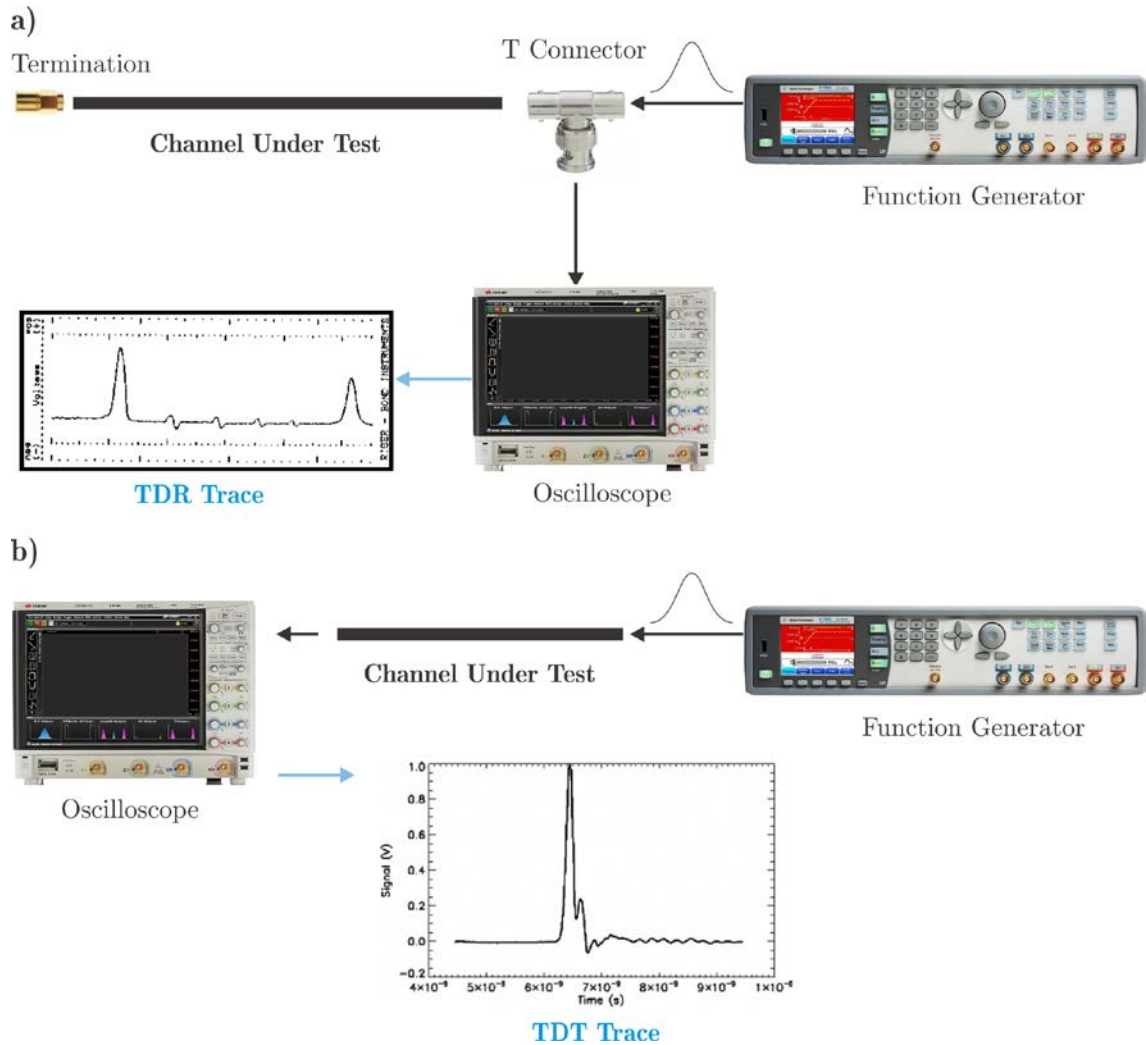


**Figure 15 – Time domain measurements scenario: reflectometry profile acquisition (a) and transmissometry profile acquisition (b).**

Both methods are applied using three pulse width configurations: 1.5 ns, 5 ns and 10 ns, so that it is possible to compare the results between their traces and evaluate the advantages and disadvantages on changing the pulse width. The other characteristics of the pulses keep the same: high level in 5 V and low level in 0 V, rise and fall time set to the minimum possible by the instrument (1 ns). For these acquisitions there is no need for a calibration process. Both TDR and TDT profiles of the channel are acquired considering both directions, or both perspectives of propagation. TDR profiles obtained from port 1 are designated as direct perspective, and from port 2 as reverse perspective. For TDT profiles, the direct perspective

designates the transmission from port 1 to port 2, and the reverse one the contrary. Each set is acquired and saved into a csv file.

## 4 RESULTS AND DISCUSSIONS

### 4.1 CHANNEL CAPACITY IN DIFFERENT LENGTHS

#### 4.1.1 Twisted-Pair Line

The channel frequency response is extracted from the characteristic impedance and propagation constant calculated for each length set of the twisted pair line, presented in Figure 16 by dashed lines, in dB. From these data curves are fitted following the model (3.2), presented by solid lines. The black dashed lines designate the lower and upper bounds of the bandwidth of interest (1.8 MHz – 86 MHz).

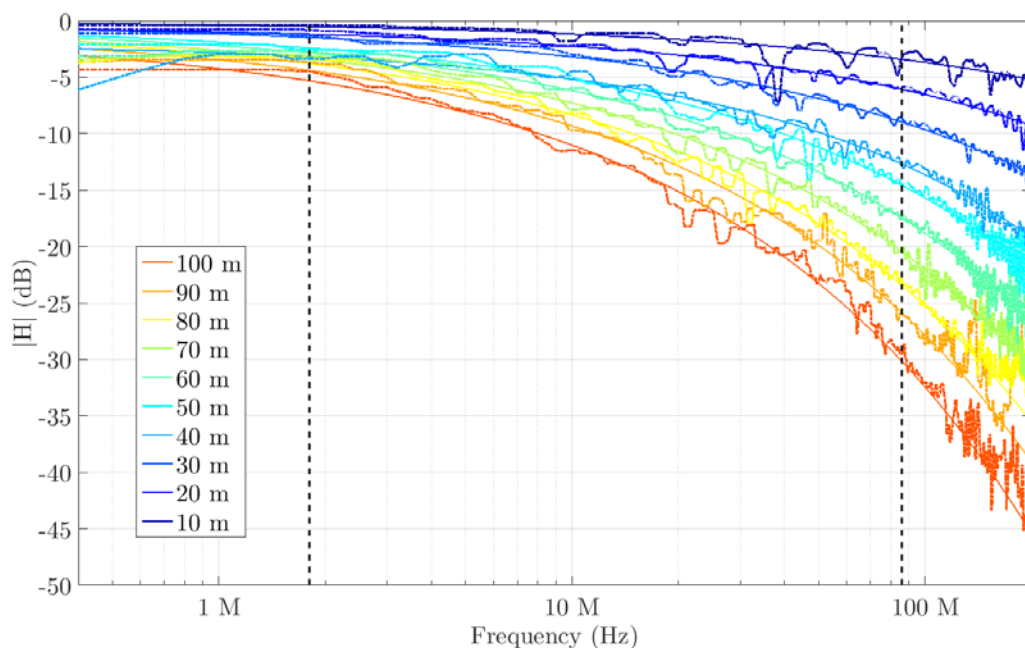


**Figure 16 - Frequency response of the twisted-pair line for the different length sets, in dB.**

Clearly, the longer the cable the lower the response will be. In this case, increasing the cable length in ten times the response decays, i.e. near at 50 MHz from -2.6 dB to -23.3 dB. These evidences reveal the influence of the length on the frequency response. For the sake of reference, a typical insertion loss for a CAT5e UTP cable is about -20 dB for a 100 meters long cable at 100 MHz (DRAKA, 2017), yet in this case verified as a lower response.

From the frequency response of the channel under analysis it is possible to accomplish the channel capacity, related to the SNR and to the bandwidth of the incident signal given by the Shannon-Hartley theorem. The channel capacity is calculated for different sets of noise level considering the bandwidth of 86 MHz, in a way that the SNR is given by the difference between the channel response at this cutoff frequency and the noise level. Thus, there will be a SNR associated to each subcarrier and length set. Noise level varies from 40 dB to 20 dB stepped in 10 dB. Besides, the performance of the communication system (PLC) operating through the cable in different lengths as channel was verified. Results are depicted in Figure 17.

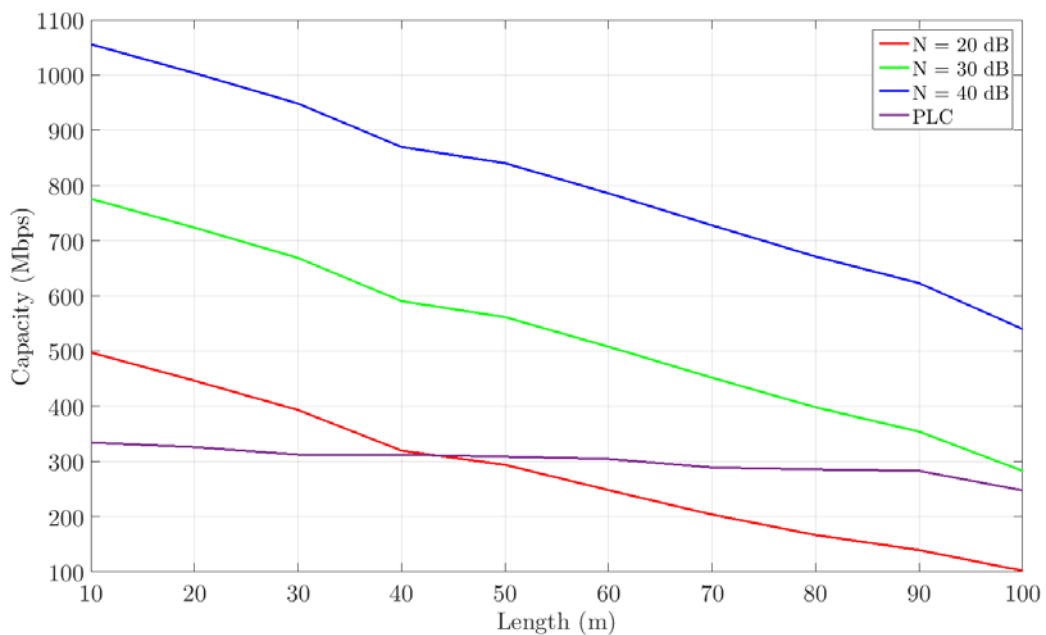


**Figure 17 - Channel capacity and performance of the twisted-pair channel.**

For a noise level of 20 dB the capacity decreases from 497.3 Mbps (10 meters long) to 102.1 Mbps (100 meters long). Capacity suffers a positive shift as the noise level decreases. For a noise level of 30 dB the capacity decreases from 775.6 Mbps to 282.8 Mbps, and for 40 dB from 1.06 Gbps to 539.7 Mbps.

Although not so explicit through the plots, the highest performance was obtained using the shortest length cable (10 m: 334.1 Mbps), and the smallest using the longer one (100 m: 247.4 Mbps). Despite the small difference between results for each length, the performance increases inversely to the length. All the performance results have kept their values below the 30 dB noise level capacities curve and crossing the 20 dB curve.

#### 4.1.2 Two-Wire Stranded Line

The channel response of the two-wire stranded  $1.5 \text{ mm}^2$  calculated is presented in Figure 18, in dB by dashed lines. Curves are fitted from these data following the model (3.2), presented by solid lines. The black dashed lines designate the lower and upper bounds of the bandwidth of interest (1.8 MHz – 86 MHz).

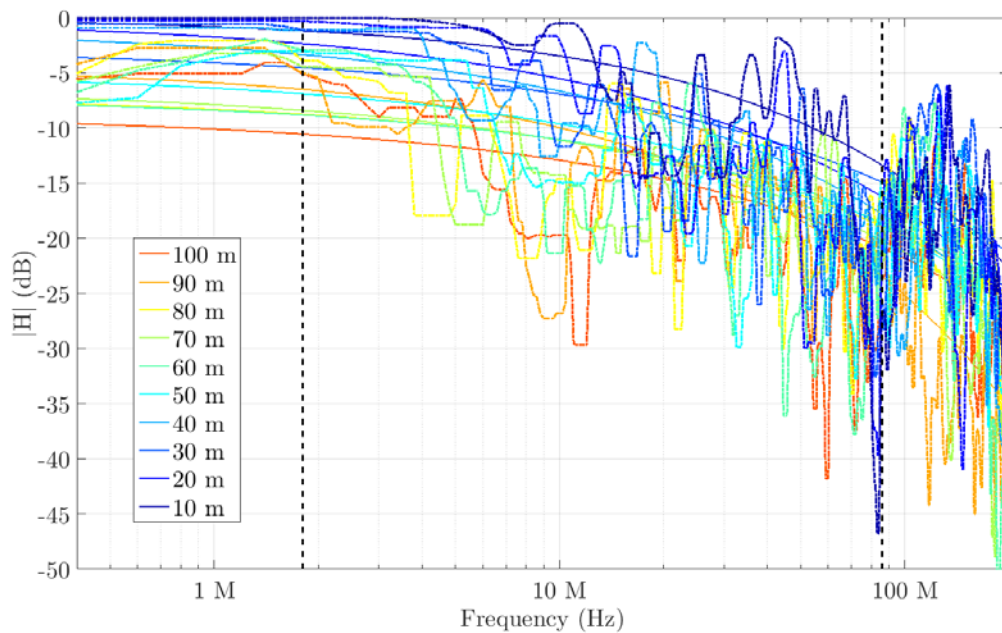


**Figure 18 - Frequency response of the two-wire line, in dB.**

The channel in all lengths sets presents a behavior not as steady over the frequency as verified through the results for the CAT5e cable. This difference may be caused by constructive aspects of both cables that leads to different electrical characteristics along the channel in space. The stranded two-wire line, for instance, does not have a constant distance between the two wires along the cable since there is not any physical tie between them, whereas the CAT5e is a twisted-pair and by definition the twists ensures periodic distance as well the outer insulation of the cable. In addition, the stranded two-wire is more susceptible to electromagnetic interference than the twisted-pair due to loop area and the absence of the twists, which brings matters to the effects of the harsh electromagnetic environment on the measurements of the scattering parameters. Despite of all these points, the cable in all sets still presents a trending behavior, stated by the decreasing of the magnitude of the response over the frequency. The response near at 50 MHz decreases from -9.5 dB in a 10 m cable to -18 dB in a 100 m cable.

Despite the decreasing trend for the whole set, there is an unexpected increasing on the response between 70 m and 80 m. This may be due to the noise level experienced when acquiring the scattering parameters and electromagnetic susceptibility of the line under test.

The channel capacity calculated for the stranded two-wire under analysis in all length sets is presented in Figure 19. The performance of the communication system using PLC devices was also verified for each cable length.

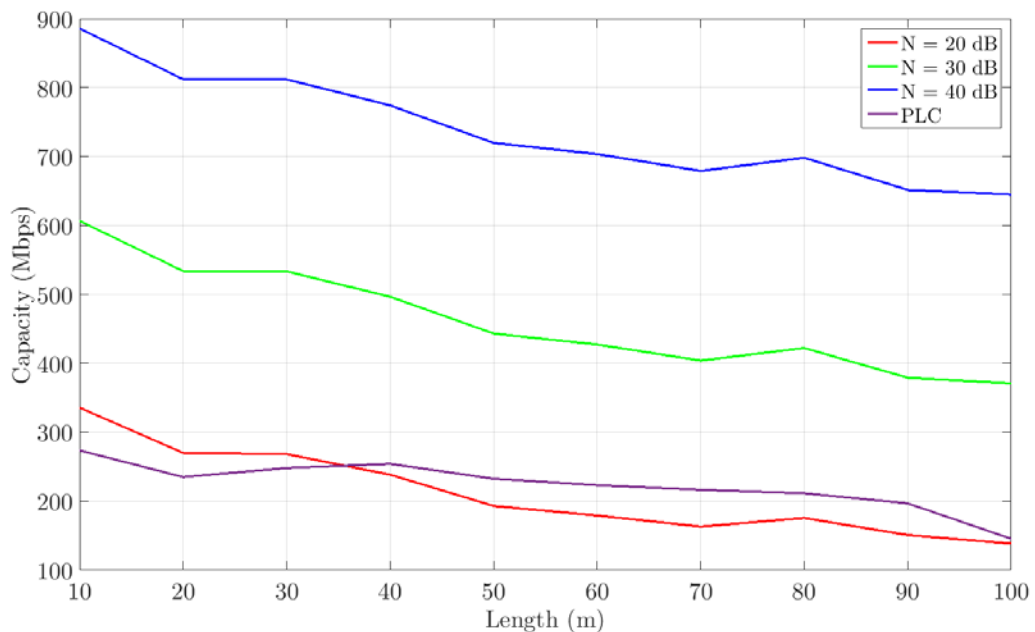


**Figure 19 - Channel capacity and performance of the two-wire channel.**

For a noise level of 20 dB, the capacity decreases from 335.4 Mbps (10 meters long) to 138.2 Mbps (100 meters long). For a noise level of 30 dB the capacity decreases from 606.5 Mbps to 370.9 Mbps, and for 40 dB from 885.8 Mbps to 644.8 Mbps.

The performance obtained with the communication system varies from 145.3 Mbps (100 m long cable) to 273.5 Mbps (10 m). The decreasing tendency is broken by the values for 20 m and 30 m, maybe due to unstable behavior of the communication system. Again, the performance results have kept below the 30 dB noise capacity curve and above the 20 dB one.

Table 1 presents a comparison between the capacities obtained for the minimum and maximum length considering the three different noise levels and communication system performance for the two types of cable evaluated.

**Table 1 - Comparison of capacities obtained for the two cables at 10 m and 100 m long.**

		Capacity (bps)			
	Length	PLC	40 dB	30 dB	-20 dB
<b>UTP</b>	<b>10 m</b>	334.1 M	1.06 G	775.6 M	497.3 M
	<b>100 m</b>	247.4 M	539.7 M	282.8 M	102.1 M
<b>Two-wire 1.5 mm<sup>2</sup></b>	<b>10 m</b>	273.5 M	885.8 M	606.5 M	335.4 M
	<b>100 m</b>	145.3 M	644.8 M	370.9 M	138.2 M

## 4.2 CHANNEL ANALYSIS IN TIME AND FREQUENCY DOMAIN

This section presents the analysis of the chosen channel, going from the time domain to frequency domain approach as described on the methodology.

### 4.2.1 Time Domain Results

First, it is extracted the TDR profile of the channel under analysis from both perspectives, starting with the direct perspective applying a pulse in the port one and monitoring the reflected signals also in this port. The reverse perspective is related to applying a pulse and monitoring the reflected signals in port two. The TDR profile for both perspectives are extracted in three pulse width configurations (1.5 ns, 5 ns and 10 ns), and for each one of them the far end of the channel connected to three termination types (open circuit, short circuit and load 50  $\Omega$ ), totalizing 9 traces for each perspective. Results for the direct perspective are depicted in Figure 20.

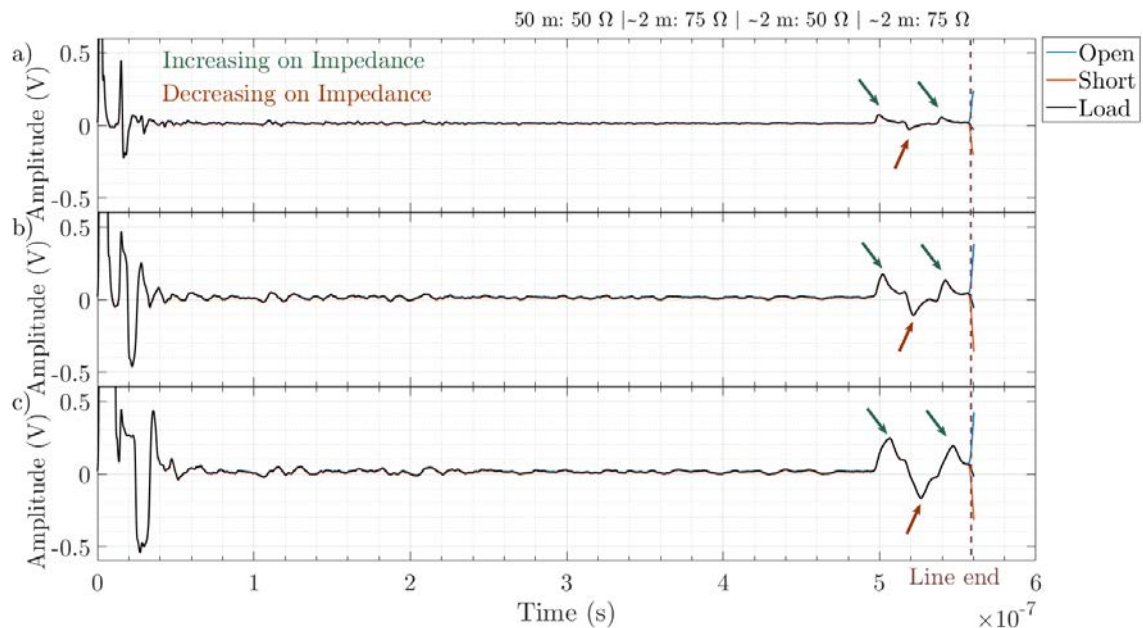


**Figure 20 - TDR profiles of the channel under test in direct perspective using different pulse widths and different terminations. (a) presents the profiles obtained with the pulse 1.5 ns wide for open, short and load termination, (b) the profile obtained with the pulse 5 ns wide for each termination, and (c) the profiles using the pulse 10 ns wide. The y axis represents the magnitude of the reflection coefficients along the channel over time.**



The end of the channel is given by the right time in the trace where the magnitude of reflection for the short termination starts to assume different value in comparison to the one using open circuit termination. For this case this event occurs at about 557 ns. Considering the round trip of the incident/reflected signal, this channel is 278.5 ns long.

On a first look at the profiles acquired for each pulse width set, it is clear a similarity on shape and time between the traces. The initial variations read vary in amplitude and dispersion. Knowing the channel and the disposition in which the sections are through this perspective, there is no possibility to associate them with any transition on the channel. The first transition for this perspective only occurs after 100 m (near at 500 ns) of round trip. Correlating the three profiles acquired, an initial increasing on the reflection coefficient is observed at 13 ns. After that, a decreasing followed by an increasing, but for these two there is no correlation in time between the profiles. For each profile they differ by amplitude, time and dispersion. These evidences may lead to correlate these initial variations to effects of the incident pulse over the channel. Narrowing the pulse these effects are compressed in time and amplitude, as can be verified.

The transitions between the sections can be verified at the far end of the channel through this perspective. The reflection coefficient increases near at 497 ns, decreases at 516 ns and increases back near at 537 ns, for the three cases.

It is evident the effect of resolution given by the pulse width difference. The narrower the pulse, the higher the resolution obtained. The resolution for the 1.5 ns trace for example is about 0.75 ns, which converted into space domain considering the velocity of propagation of 66 % of the speed of light is equal to approximately 0.15 m. For 5 ns wide, resolution will be 2.5 ns (0.495 m). For 10 ns wide, resolution is 5 ns (0.99 m). Therefore, narrower pulses will lead to a more accurate analysis, as can be verified in results through the shapes of changes on reflection coefficient at the end of the channel for example. These shapes are more defined on the 1.5 ns traces, as their changes are more abrupt in time. In other hand, narrowing the pulse comes with the decreasing on its energy. The attenuation and distortion suffered by the pulse traveling in round trip along the channel may lower its amplitude in a way which the reflections cannot be identified at the reading end. In this case, the channel is short enough to identify all the ones that matter, even for the narrowest pulse applied (1.5 ns). However, for longer channels that would be a concern. This illustrates the trade-off on choosing the pulse width and amplitude when applying reflectometry based methods.

Comparing the amplitudes for the first reflection near at 497 ns and referring to the amplitude of the reflection coefficient for 10 ns, for example, for 1.5 ns is 29.38 % and for 5 ns is 71.92 %. Results for the reverse perspective are depicted in Figure 21.

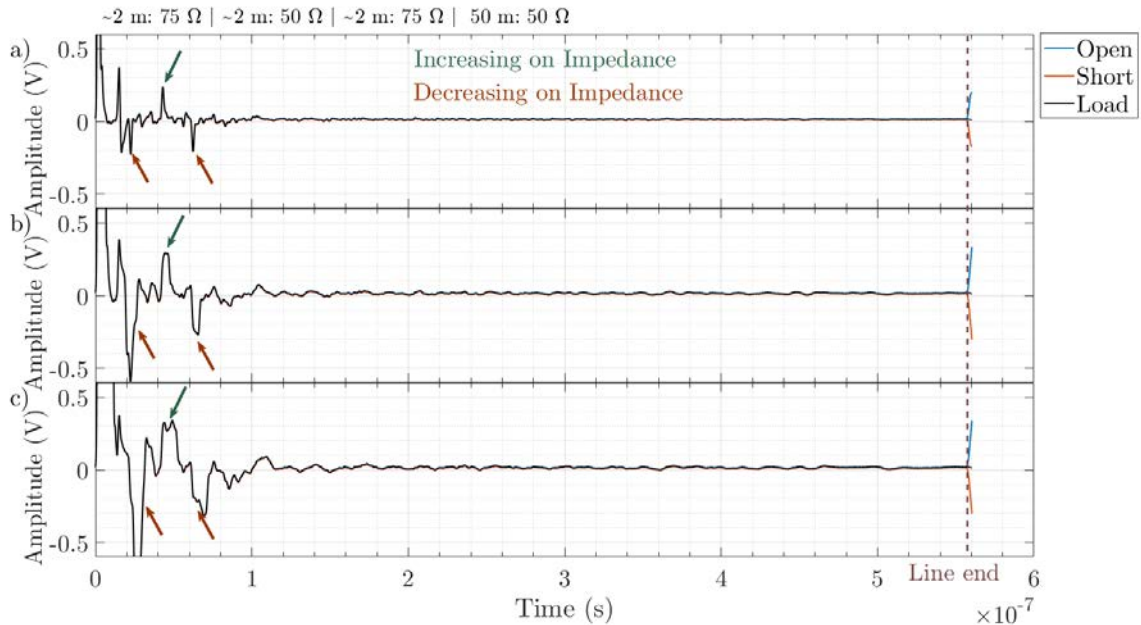


**Figure 21 - TDR profiles of the channel under test in reverse perspective using different pulse widths and different terminations. (a) shows the profiles obtained with the pulse 1.5 ns wide for open, short and load termination, (b) the profile obtained with the pulse 5 ns wide for each termination, and (c) the profiles using the pulse 10 ns wide. The y axis represents the magnitude of the reflection coefficients along the channel, given in time (x axis).**

The end of the channel is clearly verified for all the three profiles, and it converges with the end found through the direct perspective, at 557 ns. That is another evidence to state that the channel under test is about 278.5 ns long.

The profiles on this perspective reveal mean reflection coefficients at the near end, just as the sections are disposed along the channel, yet not as clearly evident as they were on the direct profile. The effects of the incident pulse applied to the channel may mask reflections at the near end, becoming worse for wider pulses since the transitory time is longer in these cases. In this case, it is verified an overlap of the incident pulse over the first transition, which can only be verified explicitly on the profiles obtained with the pulse 1.5 ns wide, at 21 ns. For the other two this transition is masked by the first decreasing on amplitude read, changing the time at which is identified at 19 ns for the pulse 5 ns wide and at 21.7 ns for the 10 ns wide one.

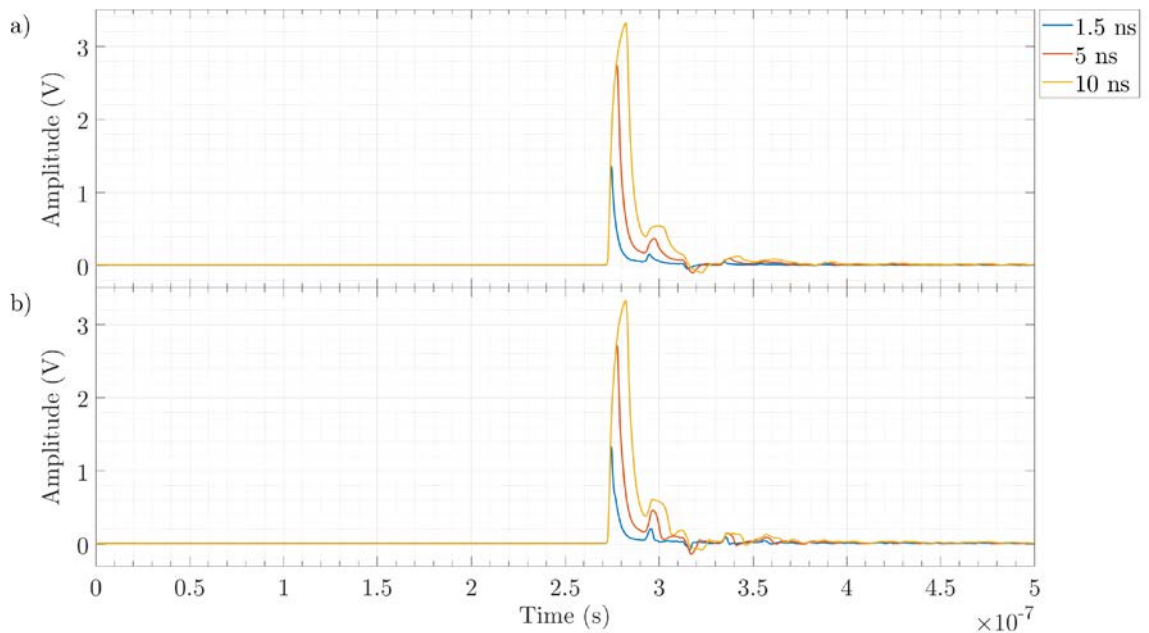
Table 2 presents the correlation between results of the analysis from both perspectives.

Table 2 - Correlation between reflections of TDR profiles in both perspectives.

Perspective		Direct			Reverse			
Section	Duration	Amplitude			Duration	Amplitude		
		1.5 ns	5 ns	10 ns		1.5 ns	5 ns	10 ns
<b>50 <math>\Omega</math> / 50.12</b> <b>m</b>	499.5 ns	0	0	0	497.5 ns	0	0	0
<b>75 <math>\Omega</math> / 1.97</b> <b>m</b>	19 ns	0.072	0.175	0.246	19.3 ns	-0.207	-0.27	-0.31
<b>50 <math>\Omega</math> / 2.03</b> <b>m</b>	21.3 ns	-0.031	-0.111	-0.17	20.5 ns	0.235	0.294	0.326
<b>75 <math>\Omega</math> / 2.07</b> <b>m</b>	20.1 ns	0.054	0.132	0.192	22.6 ns	-0.230	-0.579	-0.829

It is verified a good agreement between the time for each section in both perspectives, yet the difference verified for the maximum amplitude. The amplitude difference is related to the distortion which the pulse suffers along the channel. The pulse reflected at the near end of the channel will suffer a smaller attenuation than the one reflected at the far end of the channel.

The analysis of the channel in time domain is also made by evaluating its impulse response, thus composing the time domain transmissometry analysis. TDT is also performed considering both perspectives of the channel. Results are shown in Figure 22.



**Figure 22 - Impulse response of the channel under analysis. (a) depicts the response considering the propagation through the direct perspective, while (b) for the contrary perspective.**

The pulse takes about 272 ns to travel down the channel in both perspectives, verified by the time in which the first pulse starts rising. It conflicts with the half time for round trip achieved through the TDR analysis in both perspectives (278.5 ns), resulting in a relative error of 2.33 %. The following pulses are related to second order reflections, generated by reflections of the reflected signal over the transitions backward propagating. Since the signal generator and the oscilloscope probe have an input impedance of  $50 \Omega$ , all the signals after the first pulse are generated by internal reflections in the channel. This way what matters from this analysis is verifying how long is the line and how distorted will be an incident pulse by the channel.

There is no clear difference verified comparing the impulse response acquired from each perspective. Shape and amplitude over the time compound almost the same response. The only differences noticed are related to the amplitudes comparing the profiles obtained by different pulse widths for the same perspective. The attenuation suffered by the channel is higher for narrower pulses, as already experimented in the TDR profiles acquired. Taking the maximum amplitude acquired on the TDT profile generated by the pulse 10 ns wide as 100 % (3.32 V), the 5 ns wide response has reached 82.53 %, and 40.96 % for the 1.5 ns wide one. The difference is notable and may be related to the attenuation over the frequency components for each pulse width set. Narrower pulses have more high frequency components than the wider ones, and since

the frequency response of any channel tends to present a low-pass behavior, the high frequency components will suffer more attenuation.

#### 4.2.2 Frequency Domain Results

The following results compose the complete analysis of the channel from the scattering parameters acquired, in frequency domain. The parameter  $S_{21}$  acquired is shown in Figure 23.

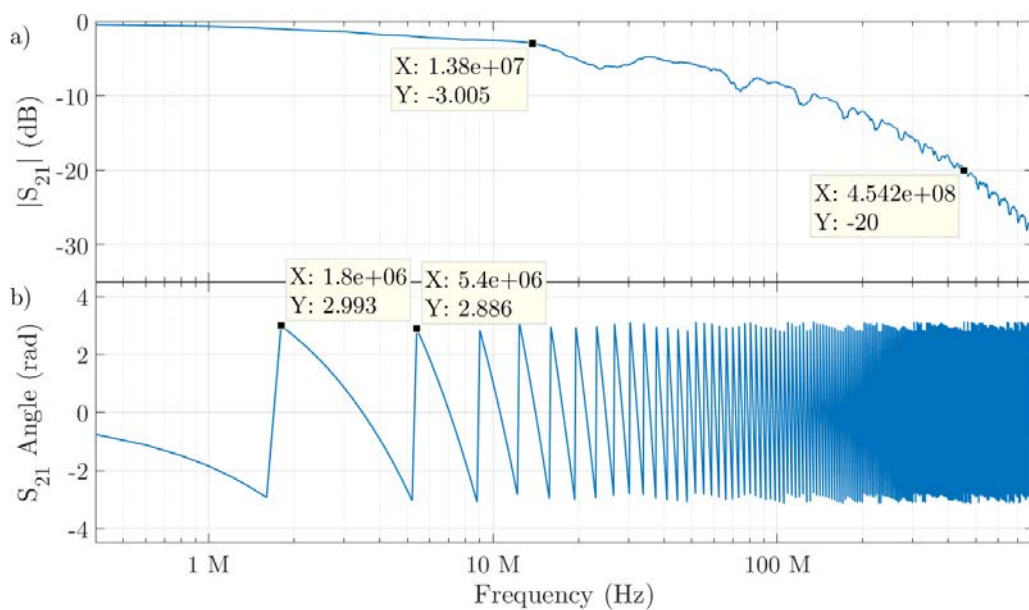


**Figure 23 -  $S_{21}$  parameter acquired for the analysis of the channel under test. (a) depicts the magnitude of the parameter, in dB. (b) presents its angle over the frequency, in rad.**

The attenuation in -3 dB occurs near at 13.8 MHz. At 100 MHz the insertion loss is -8.24 dB, and it reaches -20 dB at 454.2 MHz. The shape acquired leads to state a low-pass filter behavior, as expected for the channel. Now analyzing the insertion loss angle, a periodic response is clearly verified. This period is related to the length of the channel under analysis. In this case, the period is about 3.6 MHz, which represents the total delay of approximately 277.78 ns. Therefore, this value configures the length in time of the channel under analysis.

Figure 24 presents the  $S_{11}$  parameter acquired. Impedance matching can be verified over almost all the spectrum acquired, except at some specific ranges like 2 MHz – 10 MHz, 14 MHz – 34 MHz, and 67 MHz – 82 MHz, being more expressive in the second range described with its maximum value in -9.49 dB at 24 MHz. The matching is

related to the impedance of the measurement system, which is  $50 \Omega$  in this case. At the remaining spectrum the return loss parameter is under  $-20$  dB.

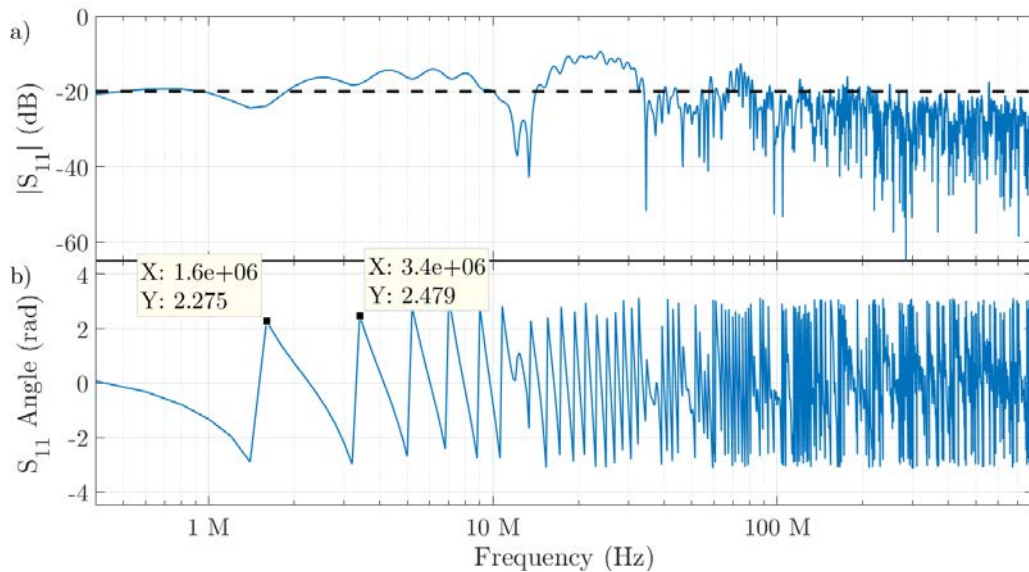


**Figure 24** –  $S_{11}$  parameter acquired for the analysis of the channel under test. (a) depicts the magnitude of the parameter, in dB. (b) presents its angle over the frequency, in rad.

The analysis of the channel length is also possible through the periodic behavior of the  $S_{11}$  angle, but now the round trip must be considered. The period verified is  $1.8$  MHz, which converted into time is about  $555.56$  ns. The channel length in time is half this value,  $277.78$  ns, which is exactly the same time found by the analysis of the periodic behavior of the  $S_{21}$  parameter.

Results of the conversion of the scattering parameters into time domain data are presented in the two following figures, being the Figure 25 related to the parameters  $S_{11}$  and  $S_{22}$  in time domain (reflection behavior) and Figure 26 to the parameters  $S_{21}$  and  $S_{12}$  in time domain (transmission behavior). Both figures present results of the conversion performed by ICZT and Sparse ICZT in comparison to time domain profiles acquired using the  $1.5$  ns wide pulse. The choice of the pulse width profiles was made considering their higher resolution in comparison to the other ones acquired. A scaling factor of  $0.143$  in amplitude was applied to the TDR signals to enable a better viewing scenario for the comparison with ICZT and Sparse ICZT results. It is important to remember that the TDR signals are purely voltage signals created by the reflection of the incident pulse, whereas ICZT and Sparse ICZT are normalized coefficients generated by the conversions.

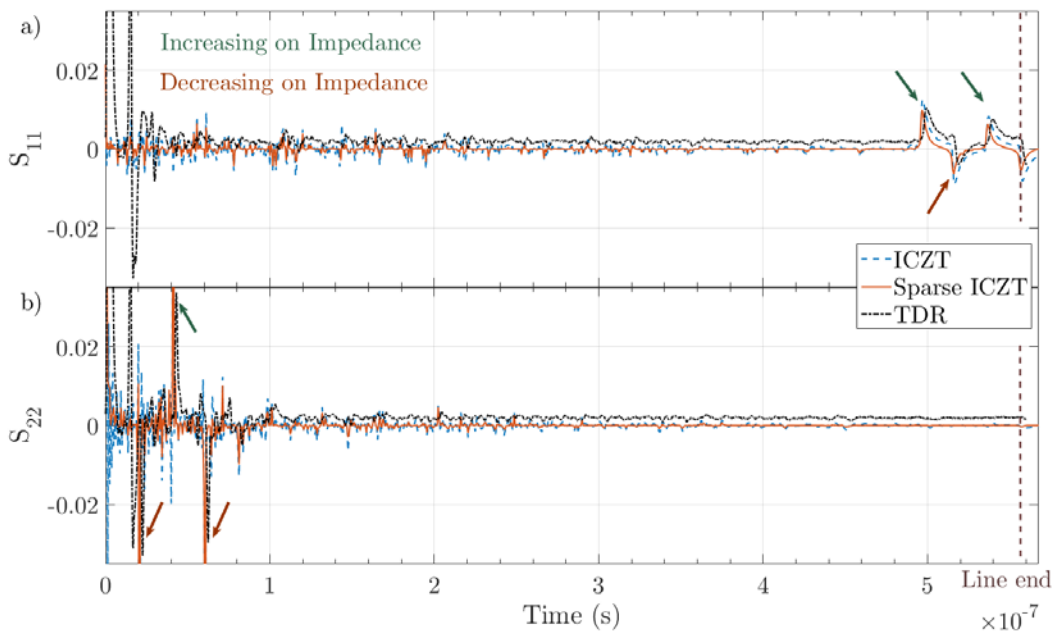


**Figure 25** – Analysis of the parameters  $S_{11}$  and  $S_{22}$  in time domain, given by the conversion performed by ICZT and Sparse ICZT, in comparison to the TDR profile acquired. (a) is related to the direct perspective of the channel, whereas (b) to the reverse perspective.

Analyzing the conversion of the parameter  $S_{11}$  in time domain, it is possible to verify four transitions along the channel, all of them concentrated at the far end of the channel. The first transition happens near at 496 ns, corresponding to an increasing on the characteristic impedance. Then, after 20 ns a second transition designated by a decreasing on it. Following the signal, after 20 ns there is an increasing on the characteristic impedance representing the third transition. The last transition, near at 557 ns, represents a decreasing one. Correlating these results with the channel under analysis, the transitions are verified just as the sections are disposed in time / length along the channel through this perspective, as well the change tendencies on the characteristic impedance. The last transition corresponds to the end of the channel, which is the border between the section with characteristic impedance in  $75 \Omega$  and the network analyzer input impedance of  $50 \Omega$ . That is why its magnitude is similar to the one related to the transition from second to third section ( $75 \Omega$  to  $50 \Omega$ ).

Now analyzing the parameter  $S_{22}$  in time domain, three transitions are clear to identify at the near end: a decreasing near at 21 ns, an increasing near at 41 ns, and a last decreasing near at 61 ns. The transitions are disposed just as the sections are in the channel through the reverse perspective. In this case, the magnitudes are higher than the ones obtained from the other perspective. The network analyzer equipment

acquires the parameters at one frequency at a time. Since the channel behaves as a low pass filter, each frequency component of the interrogator signal will suffer a different attenuation. Moreover, there is also the attenuation over the channel length. That is why the same section transitions have presented different amplitudes comparing the scattering parameters acquired for each perspective converted to time domain.

For both perspective profiles given by the conversion of the scattering parameters  $S_{11}$  and  $S_{22}$  it is verified a good agreement in shape and time between results obtained by ICZT and Sparse ICZT. The most explicit difference is related to the amplitude, with an average difference in about 77.04 %, Sparse ICZT referred to ICZT.

Table 3 presents a comparison between the transition times in profiles obtained with the conventional ICZT and the Sparse ICZT method, as well the correlation between the duration for each section through each perspective. It is also presented information about the TDR profiles acquired, in a way to compare them with their respective scattering parameters converted into time domain.

**Table 3 - Correlation between the scattering parameters  $S_{11}$  and  $S_{22}$  in time domain, obtained by ICZT and Sparse ICZT, and TDR profiles.**

Perspective		Direct ( $S_{11}$ )			Reverse ( $S_{22}$ )		
Section		ICZT	Sparse ICZT	TDR 1.5 ns	ICZT	Sparse ICZT	TDR 1.5 ns
<b>50 <math>\Omega</math> / 50.12</b>	<b>Transition at</b>	496.6 ns	496.6 ns	499.5 ns	556.6 ns	556.6 ns	559.9 ns
	<b>m</b>						
	<b>Length</b>	496.6 ns	496.6 ns	499.5 ns	496 ns	496 ns	497.5 ns
<b>75 <math>\Omega</math> / 1.97</b>	<b>Transition at</b>	516.6 ns	516 ns	518.5 ns	60.6 ns	60.6 ns	62.4 ns
	<b>m</b>						
	<b>Length</b>	20 ns	19.4 ns	19 ns	19.4 ns	19.4 ns	19.3 ns
<b>50 <math>\Omega</math> / 2.03</b>	<b>Transition at</b>	537.2 ns	536.5 ns	539.8 ns	41.2 ns	41.2 ns	43.1 ns
	<b>m</b>						
	<b>Length</b>	20.6 ns	20.5 ns	21.3 ns	20.6 ns	20.6 ns	20.5 ns
<b>75 <math>\Omega</math> / 2.07</b>	<b>Transition at</b>	557.8 ns	556.6 ns	559.9 ns	20.6 ns	20.6 ns	22.6 ns
	<b>m</b>						
	<b>Length</b>	20.6 ns	20.1 ns	20.1 ns	20.6 ns	20.6 ns	22.6 ns

Correlating the sections identified through each perspective, the maximum difference for time duration of each one is about 0.6 ns for ICZT and Sparse ICZT conversions, and 2.5 ns for TDR profiles, which correspond in length to 3 cm and 12.4 cm respectively. These errors represent 0.05 % and 0.022 % of total the length of the channel under analysis, revealing the good correlation between the scattering



parameters  $S_{11}$  and  $S_{22}$  in time domain, and between the TDR profiles. In other words, that states the similarity between the perspective profiles.

It is possible to verify a delay in ICZT and Sparse ICZT signals referred to the TDR profiles, with an average value of 3 ns for the direct perspective and 2.25 ns for the reverse one. Although the differences, there is a good agreement in shape of the signals.

Taking as reference the results of the conversion performed by ICZT, the maximum difference for the transition times for the direct perspective is about 1.2 ns for Sparse ICZT method and about 2.9 ns for TDR. For the length times is about 0.6 ns and 2.9 ns respectively. Now analyzing the reverse perspective, no difference between Sparse ICZT and ICZT transition times and length times was verified. For TDR a maximum difference of 3.3 ns in transition times and 2 ns in length times. Table 4 presents the maximum relative errors listed in percentage values.

**Table 4 - Maximum relative errors for the correlation between the scattering parameters  $S_{11}$  and  $S_{22}$  in time domain, obtained by ICZT and Sparse ICZT, and TDR profiles, taking ICZT method as reference.**

Relative error (%)	Direct		Reverse	
	Sparse ICZT	TDR 1.5 ns	Sparse ICZT	TDR 1.5 ns
Transition time	0.2	0.6	0	9.7
Length time	3	5	0	9.7

Errors values reveal promising performance of the Sparse ICZT and limitations on TDR measurements considering resolution over acquiring the profiles through scattering parameters.

Results for the conversion of the scattering parameters  $S_{21}$  and  $S_{12}$  in time domain in comparison to the TDR profiles acquired are depicted in Figure 26.

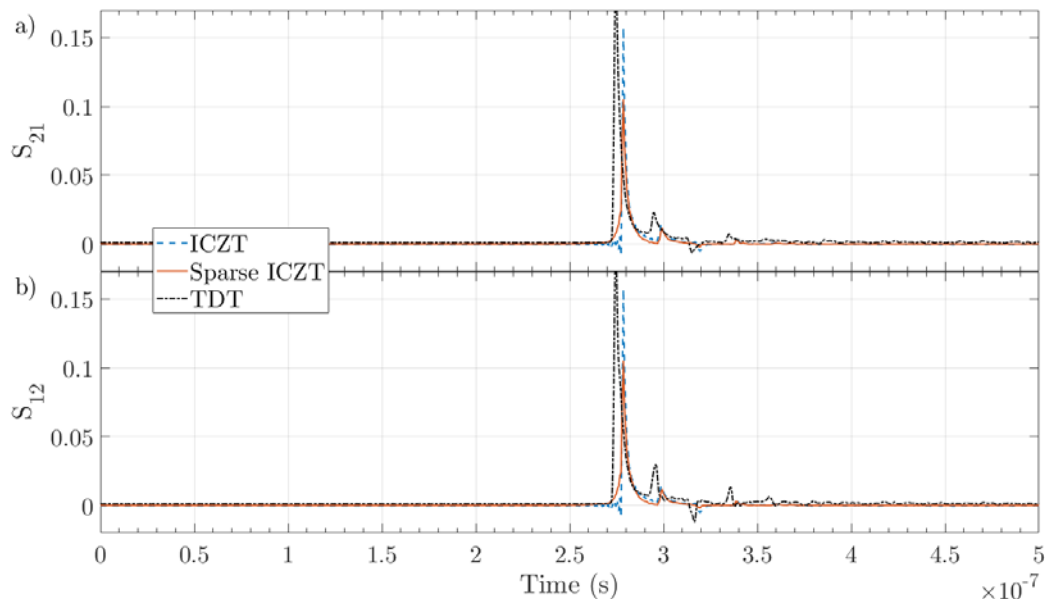
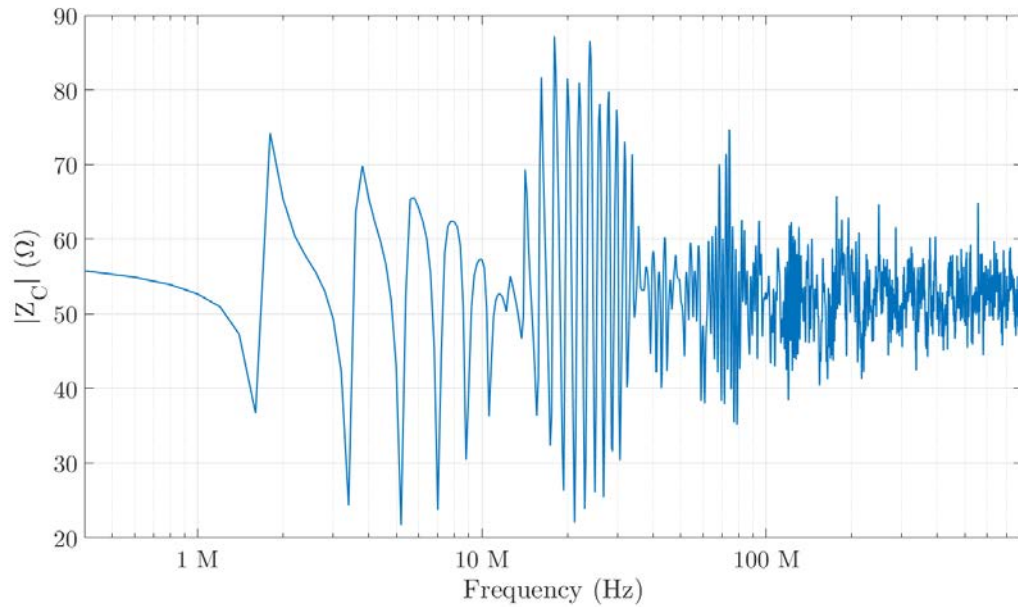


**Figure 26** - Analysis of the parameters  $S_{21}$  and  $S_{12}$  in time domain, presenting results of the conversion performed by ICZT and Sparse ICZT, in comparison to the TDT profile acquired. (a) presents the parameter  $S_{21}$  in time domain, related to the direct perspective propagation. (b) presents the parameter  $S_{12}$  in time domain, related to the reverse perspective propagation.

These parameters in time domain are related to the impulse response of the channel under analysis, revealing the delay and attenuation caused by the channel. On a first look, it is verified the similarity in behavior between them. That means that there will be no difference propagating a signal through this channel in any perspective. The delay is about 278.6 ns for both parameters  $S_{21}$  and  $S_{12}$  in time domain for both conversion methods, whereas for the TDT profiles is about 274.5 ns for both perspectives. Although, the amplitudes obtained also diverges from one to the other. The amplitude in both perspectives of the first pulse is 0.157 for ICZT, while for Sparse ICZT is 0.105. For a better comparison, a scaling factor of 0.143 in amplitude was applied to the TDT signals, remembering that they are purely voltage signals, whereas ICZT and Sparse ICZT are normalized coefficients.

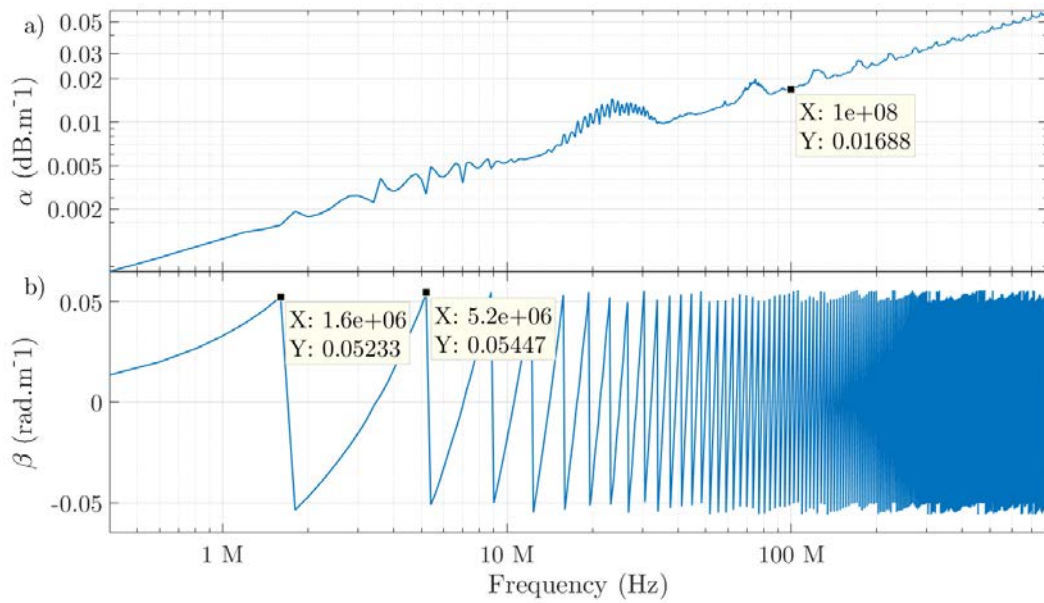
Back to the analysis of the scattering parameters in the frequency domain, first it is extracted the secondary parameters characteristic impedance and propagation constant. In Figure 27 the results for the characteristic impedance are depicted, in absolute values. The characteristic impedance also presents a periodic behavior that reveals the length of the channel under test, with period in 1.8 MHz. It varies in magnitude from 30 to 80  $\Omega$  for frequencies lower than 33.8 MHz. After that it keeps

varying between 45 and 60  $\Omega$ . Although, for the whole spectrum there is a trend value of about 55  $\Omega$  for the characteristic impedance magnitude.



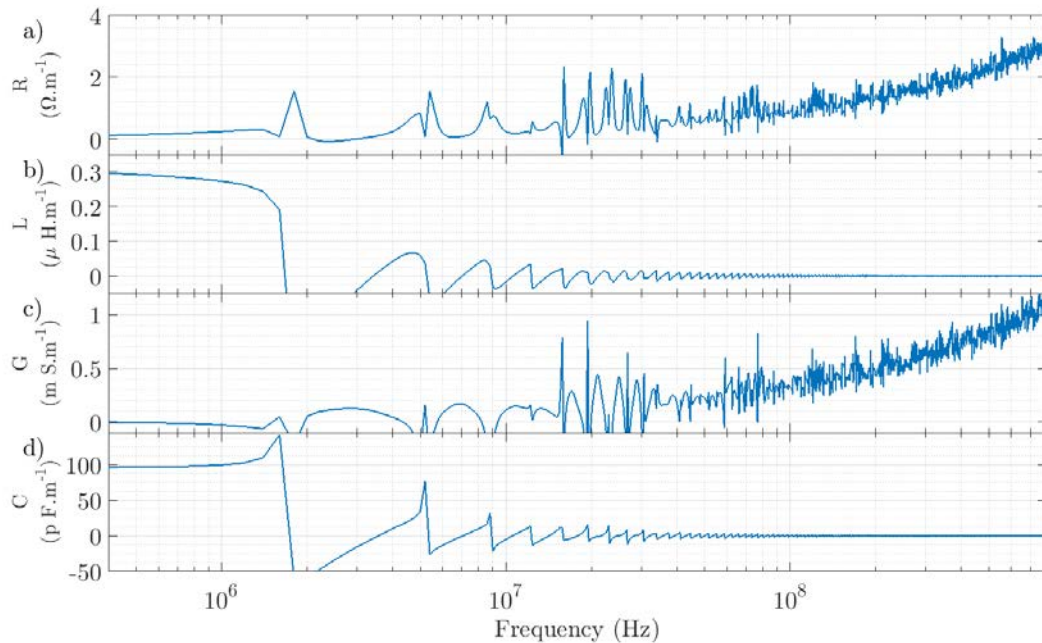
**Figure 27 - Characteristic impedance of the cascaded transmission line under analysis calculated from the scattering parameters acquired.**

Figure 28 presents the propagation constant calculated of the channel under test, being alpha the real part related to the attenuation given in  $\text{Np.m}^{-1}$ , and beta the imaginary part related to the phase constant in  $\text{rad.m}^{-1}$ . The attenuation constant increases with the frequency. At 100 MHz it reaches the value of 0.017. The phase constant varies periodically between about -0.05 and 0.05. The period, 3.6 MHz, is directly related to length of the channel, as verified in angle of the  $S_{21}$  parameter acquired.



**Figure 28 - Propagation constant calculated from the scattering parameters acquired of the mixed channel. The attenuation constant alpha (a) (real part of the propagation constant) increases with the frequency, standing near to 0.017 at 100 MHz. The phase constant beta (b) (imaginary part) varies periodically following the length of the channel under test.**

From the secondary parameters  $Z_C$  and  $\gamma$  the primary ones can be calculated. Figure 29 presents the calculated distributed parameters of the channel under analysis.



**Figure 29 - Distributed parameters calculated for the channel under analysis. (a) depicts the distributed resistance given in  $\Omega.m^{-1}$ , (b) the distributed inductance in  $\mu H.m^{-1}$ , (c) the distributed conductance in  $m S.m^{-1}$ , and (d) the distributed capacitance in  $p F.m^{-1}$ .**

The distributed resistance and conductance parameters increase exponentially with frequency. At 100 MHz, their values are in  $0.87 \Omega.m^{-1}$  and  $327 \mu S.m^{-1}$  respectively. Although some abrupt changes, it is verified a trend behavior on the increasing.

The distributed inductance and capacitance parameters decrease with the frequency. Their values start in about  $300 nH.m^{-1}$  and  $100 pF.m^{-1}$  respectively. At 100 MHz the distributed inductance is  $0.69 n H.m^{-1}$  and distributed capacitance is  $0.21 pF.m^{-1}$ .

Now looking forward to verify the channel response, from the propagation constant and length it is possible to achieve it as depicted in Figure 30.

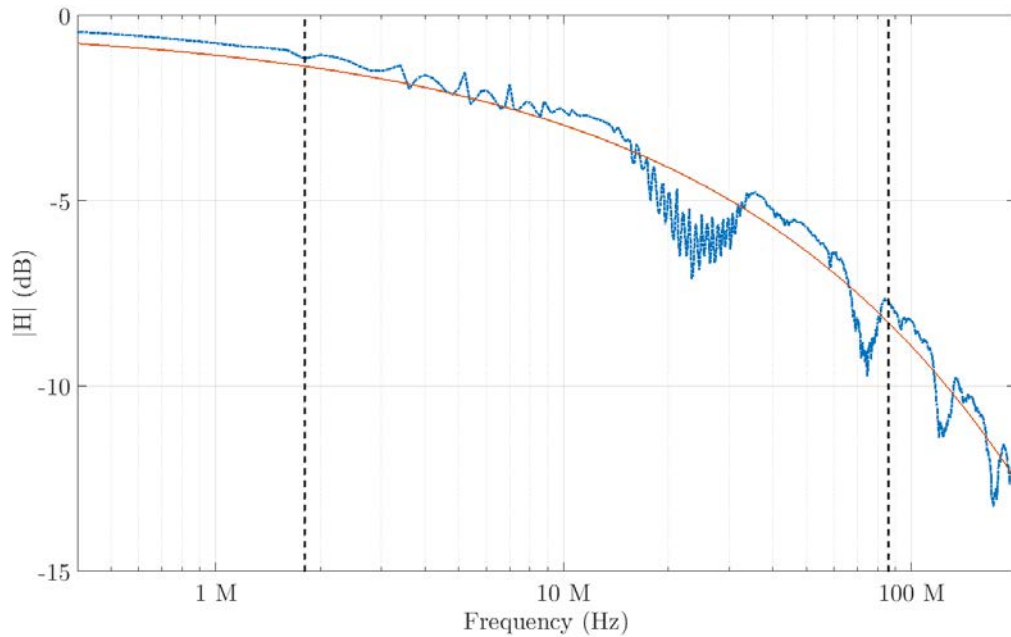


**Figure 30 - Frequency response of the channel under analysis, in dB.**

Following the same analysis done for the channel capacity in function of length, a new function for the channel response is fitted from calculated channel response. The function is defined at the bandwidth 1.8 MHz – 86.13 MHz, with 3455 subcarriers equally spaced in 24.414 kHz. The channel capacity is calculated in function of noise level referred to the signal level (fitted channel response), following the Shannon-Hartley's theorem. Noise levels are 20 dB, 30 dB and 40 dB. Results are depicted in Table 5.

**Table 5 - Channel capacity (Mbps) calculated in function of the channel frequency response and noise level.**

Noise (dB)	Channel capacity (Mbps)
20	405.5
30	681.4
40	961.2

## 5 CONCLUSIONS

Electrical cable networks are widely employed for energy distribution and communication systems. In many applications, such cables are exposed to harsh environments. Subsea systems in the oil industry are a typical example. The demand for maximum power transfer, less susceptible to electromagnetic interference and greater transmission rates requires the analysis of the transmission lines parameters in details and continuously.

In this work a study of techniques for analysis of transmission lines in time and frequency domain is presented. To evaluate the influence of length on the channel capacity, the capacity was obtained from scattering parameters of an unshielded twisted pair CAT5e in ten different lengths. Here the assumption that the signal level is limited by the bandwidth of 1.8 MHz to 86 MHz was taken, following the HomePlug AV2 specifications, which was taken as commercial example of communication system for the sake performance evaluation. Results are curves of the channel capacity for different noise levels in function of length. From them it is possible to evaluate the maximum rates for each length in different SNR conditions. The same experiment was done using a two wire stranded copper 1.5 mm<sup>2</sup> cable. Due to its constructive characteristics the scattering parameters acquired has presented an unstable behavior in comparison to the other cable. Although, for both kinds it is verified the relationship between the length and maximum capacity. For both cables it was verified a performance beyond the 20 dB noise level capacity curve and below the 30 dB curve, suggesting the PLC working noise level.

Looking forward to understand techniques for the analysis of transmission lines in time and frequency domain, a set of analysis for a chosen transmission line configuration is also proposed, composed by four sections of coaxial cables with different lengths and characteristic impedance alternating between 50  $\Omega$  and 75  $\Omega$ . The analysis started in time domain with the extraction of TDR and TDT profiles of the channel, for both perspectives of reflection and transmission respectively, and in three different pulse width configurations. Through the results it was observed the effects of trade-off between pulse width and amplitude over the profile resolution. The narrower the pulse the greater the resolution, even though the energy decreasing by it also implies a decreasing on the energy of the reflected pulse and might cause its vanish. The analysis

of the profiles acquired allows the verification of type and location of impedance transitions along the line, as well its length and impulse response.

The analysis of the channel under test in frequency domain starts with the extraction of the scattering parameters. From them it is calculated the secondary parameters of the line characteristic impedance and propagation constant. These parameters reveal the behavior of the channel over the frequency spectrum acquired, and knowing its length lead to the primary ones: distributed resistance, inductance, conductance and capacitance.

From scattering parameters it is also possible the analysis of the channel in time domain, given by the Inverse Chirp Z Transform. In this work, a sparse approach for this inverse problem is also proposed, since the nature of the impedance mismatches along a transmission line is sparse. Results of the conversion solved by the proposed method are compared to the ones obtained by the conventional Inverse Chirp Z Transform. Through the comparison, it is verified a good agreement in time location and wave shape of the signals, revealing promising results in time domain analysis of scattering parameters.

## 5.1 FUTURE WORK

The presented work opens horizons to the development of more complex and detailed studies on techniques for characterizing channels field. It is suggested the application of the proposed sets of experiment using a real network managed by a real communication system, in a way to achieve the maximum capacity at the environment in which the system runs. This will require the study in details of proper noise models and of the technology used by the system modems.

Moreover, on the channel characterization in time and frequency domain, it is suggested an investigation and application of more complex methods for obtaining the impedance profile of the line, so that the reflections coefficients can be achieved purely, with no influence of second order reflections. In addition, the performance of the proposed method Sparse Inverse Chirp Z Transform for time domain analysis of transmission lines must be evaluated, being suggested to be compared to the conventional Inverse Chirp Z Transform method.



## REFERENCES

AGILENT TECHNOLOGIES. **S-Parameter Design - Application note 154**, 2006.

AGILENT TECHNOLOGIES. **Time Domain Analysis Using a Network Analyzer - Application note 1287-12**, 2012.

AGILENT TECHNOLOGIES. **Time Domain Reflectometry Theory - Application note 1304-2**, 2013.

ALLIANCE, P.; RESERVED, A. R. HomePlug AV White Paper. **Architecture**, p. 1–11, 2005.

ALLIANCE HPGP. HomePlug™ AV2 technology. **HomePlug Powerline Alliance, Inc**, p. 1–12, 2013.

ANRISTU. **A Guide to Making RF Measurements for Signal Integrity Applications**, 2016.

BAHAI, A. R. S.; SALTZBERG, B. R.; ERGEN, M. **Multi-Carrier Digital Communications: Theory and Applications of OFDM**. Second ed. Springer, 2004.

BECK, A.; TEBOULLE, M. Fast Gradient-Based Algorithms for Constrained Total Variation Image Denoising and Deblurring Problems. **IEEE Transactions on Image Processing**, v. 18, n. 11, p. 2419–2434, 2009a.

BECK, A.; TEBOULLE, M. A Fast Iterative Shrinkage-Thresholding Algorithm. **Society for Industrial and Applied Mathematics Journal on Imaging Sciences**, v. 2, n. 1, p. 183–202, 2009b.

BEGOVIC, A.; SKALJO, N.; GORAN, N. **An example of estimation of twisted pair channel capacity in DSL environment.** 1st International Conference on Communications, Signal Processing, and their Applications (ICCSPA). IEEE, feb. 2013

BLEMEL, K.; FURSE, C. **Applications of microsystems and signal processing for wiring integrity monitoring.** 2001 IEEE Aerospace Conference Proceedings (Cat. No.01TH8542). IEEE, 2001

CHING-WEN HSUE; TE-WEN PAN. Reconstruction of nonuniform transmission lines from time-domain reflectometry. **IEEE Transactions on Microwave Theory and Techniques**, v. 45, n. 1, p. 32–38, 1997.

DE PORRATA-DORIA I YAGUE, R.; IBARS, A. B.; MARTINEZ, L. F. Analysis and reduction of the distortions induced by time-domain filtering techniques in network analyzers. **IEEE Transactions on Instrumentation and Measurement**, v. 47, n. 4, p. 930–934, 1998.

DRAKA. **UC300 24 Cat.5e Datasheet**Draka Prysmian Group, , 2017. Available on: <[https://www.prysmiangroup.com/sites/default/files/business\\_markets/markets/downloads/datasheets/da13e\\_0.pdf](https://www.prysmiangroup.com/sites/default/files/business_markets/markets/downloads/datasheets/da13e_0.pdf)>

DUNSMORE, J.; CHENG, N.; ZHANG, Y. **Characterizations of asymmetric fixtures with a two-gate approach.** 77th ARFTG Microwave Measurement Conference. IEEE, jun. 2011

EZZINE, S. et al. Evaluation of PLC channel capacity and ABER performances for OFDM-based two-hop relaying transmission. **Wireless Communications and Mobile Computing**, 2017.

FRANCIS, A.; TITUS, G. **Channel capacity analysis of railway power lines.** 2011 International Conference on Emerging Trends in Electrical and Computer Technology.

IEEE, mar. 2011

FRICKEY, D. A. Using the Inverse Chirp-Z Transform for Time-Domain Analysis of Simulated Radar Signals. **ICSPAT 94: signal procession applications and technology**, p. 1–6, 1994.

GOLDSMITH, A. **Wireless Communications**. Cambridge: Cambridge University Press, 2005.

HAYT, W. H.; BUCK, J. A. Engineering Electromagnetics. **Engineering Electromagnetics**, p. 563, 2011.

HERNANDEZ-MEJIA, J. C. **Time Domain Reflectometry**. Neetrac Georgia Tech, 2016.

IDA, N. **Engineering Electromagnetics**. Third ed. Cham: Springer International Publishing, 2015.

KOTCHASARN, C. Performance Analysis of Broadband Power Line Communications with OFDM Transmission. p. 316–320, 2017.

KWAK, K. S. et al. Reduction of the blind spot in the time-frequency domain reflectometry. **IEICE Electronics Express**, v. 5, n. 8, p. 265–270, 2008.

LAMPE, L.; TONELLO, A. M.; SWART, T. G. **Power Line Communications: Principles, Standards and Applications from Multimedia to Smart Grid**. Second ed. Chichester, UK: John Wiley & Sons, Ltd, 2016.

LIN, Y.-P.; PHOONG, S.-M.; VAIDYANATHAN, P. P. **Filter bank transceivers for OFDM and DMT systems**. First ed. Cambridge: Cambridge University Press, 2011.

MERSEREAU, R. An Algorithm for Performing an Inverse Chirp Z-Transform. **IEEE Transactions on Acoustics, Speech, and Signal Processing**, v. 22, n. 5, p. 387–388, oct. 1974.

PAPAZYAN, R. et al. Extraction of high frequency power cable characteristics from S-parameter measurements. **IEEE Transactions on Dielectrics and Electrical Insulation**, v. 11, n. 3, p. 261–270, jun. 2004.

PASTERNAK. **Flexible RG58 Coax Cable Single Shielded with Black PVC Jacket Datasheet** Pasternack Enterprises, , 2017. Available on: <<https://www.pasternack.com/images/ProductPDF/RG58C-U.pdf>>

POZAR, D. **Microwave Engineering**. Fourth ed. John Wiley & Sons, Inc., 2005.

QINGHAI SHI; KANOUN, O. Wire Fault Diagnosis in the Frequency Domain by Impedance Spectroscopy. **IEEE Transactions on Instrumentation and Measurement**, v. 64, n. 8, p. 2179–2187, aug. 2015.

QINGHAI SHI; TROLTZSCH, U.; KANOUN, O. **Analysis of the parameters of a lossy coaxial cable for cable fault location**. Eighth International Multi-Conference on Systems, Signals & Devices. IEEE, mar. 2011

RABINER, L.; SCHAFER, R.; RADER, C. The Chirp Z-Transform Algorithm. **IEEE Transactions on Audio and Electroacoustics**, v. 17, n. 2, p. 86–92, jun. 1969.

RAHMAN, M. M.; MAJUMDER, S. P. Performance analysis of a OFDM SISO powerline communication system with non-white Gaussian channel noise. **1st International Conference on Electrical Engineering and Information and Communication Technology, ICEEICT 2014**, p. 1–4, 2014.

RITO, M.-C. et al. Communications System for Down-Hole Measurements. **Journal of Applied Research and Technology**, v. 11, n. 6, p. 903–911, dec. 2013.

ROHLING, H. **OFDM. Concepts for Future Communication Systems**. Berlin, Heidelberg: Springer Berlin Heidelberg, 2011.

SHANNON, C. E. A Mathematical Theory of Communication. **Bell System Technical Journal**, v. 27, n. 3, p. 379–423, 1 jul. 1948.

SHANNON, C. E. Communication in the Presence of Noise. **Proceedings of the IRE**, v. 37, n. 1, p. 10–21, jan. 1949.

SHI, Q.; KANOUN, O. Wire fault location in coaxial cables by impedance spectroscopy. **IEEE Sensors Journal**, v. 13, n. 11, p. 4465–4473, 2013.

SMITH, P.; FURSE, C.; GUNTHER, J. Analysis of spread spectrum time domain reflectometry for wire fault location. **IEEE Sensors Journal**, v. 5, n. 6, p. 1469–1478, dec. 2005.

VAN HAMME, H. High-resolution frequency-domain reflectometry by estimation of modulated superimposed complex sinusoids. **IEEE Transactions on Instrumentation and Measurement**, v. 41, n. 6, p. 762–767, 1992.

VANHAMME, H. High resolution frequency-domain reflectometry. **IEEE Transactions on Instrumentation and Measurement**, v. 39, n. 2, p. 369–375, apr. 1990.

VEIJOLA, T. V.; VALTONEN, M. E. Identification of cascaded microwave circuits with moderate reflections using reflection and transmission measurements. **IEEE Transactions on Microwave Theory and Techniques**, v. 36, n. 2, p. 418–423, 1988.

WALSH, J. F. **Dual Time Base Zero Dead Zone Time Domain Reflectometer**. United States Patent, 1995.

WEBER, G. H. et al. **Sparse Inverse Chirp-Z Transform of S-Parameter Measurements for Time Domain Analysis of Transmission Line**. XXXV Simpósio Brasileiro de Telecomunicações e Processamento de Sinais - SBrT2017. São Pedro: 2017

YAMADA, T.; HIRAI, N.; OHKI, Y. **Improvement in sensitivity of broadband impedance spectroscopy for locating degradation in cable insulation by ascending the measurement frequency**. 2012 IEEE International Conference on Condition Monitoring and Diagnosis. IEEE, sep. 2012

YONGE, L. et al. An Overview of the HomePlug AV2 Technology. **Journal of Electrical and Computer Engineering**, v. 2013, p. 1–20, 2013.

ZYARI, M.; ROLAIN, Y. Identifying Multiple Reflections in Distributed-Lumped High-Frequency Structures. **IEEE Transactions on Microwave Theory and Techniques**, v. 64, n. 4, p. 1306–1312, apr. 2016.